IPS E.MAX CAD AND IPS E.MAX PRESS: FRACTURE MECHANICS CHARACTERIZATION

by

Lubna T. Alkadi

DDS, King Saud University, 2010

A THESIS SUBMITTED IN PARTIAL FULFILLMENT OF

THE REQUIREMENTS FOR THE DEGREE OF

MASTER OF SCIENCE

in

THE FACULTY OF GRADUATE AND POSTDOCTORAL STUDIES

(CRANIOFACIAL SCIENCES)

THE UNIVERSITY OF BRITISH COLUMBIA

(Vancouver)

July 2014

© Lubna T. Alkadi, 2014

Abstract

Objective: To determine fracture toughness (K_{IC}) and fatigue crack propagation (FCP) parameters for IPS e.max CAD and IPS e.max Press.

Materials and methods: For K_{IC} determinations, 20 (6x6x6x12mm) notchless triangular prism (NTP) specimens of IPS e.max CAD and IPS e.max Press were prepared. IPS e.max CAD blocks were cut, ground and then crystallized, while IPS e.max Press ingots were pressed into molds obtained from wax prisms. Each specimen was mounted into a holder and custom grips were used to attach the holder to a computerized universal testing machine (Instron model 4301). The assembly was loaded in tension at a crosshead speed of 0.1mm/min and K_{IC} was calculated based on the recorded maximum load at fracture. Fractured surfaces were characterized using scanning electron microscopy (SEM). The results were statistically analyzed using Weibull statistics and t-test (α=0.05).

For FCP characterization, a pilot test was done with three Plexiglas NTP samples. A pre-crack was initiated in one of the specimen edges. Several lines were scribed on the side of the specimen to monitor crack propagation. The specimens were mounted in the holder and then attached to custom grips on a servo hydraulic fatigue-testing machine (Instron model 8511). A strain gauge was attached to these grips to monitor crack opening displacement. Each specimen was cyclically loaded in tension (Mode I) in a load range between 1 and 20 N and crack length was monitored and filmed using a high definition video recorder (SONY HDR-XR550V) attached to a microscope (Edmund Scientific Co, Barrington, NJ). Video recording was terminated once catastrophic fracture of the specimen occurred. Cyberlink Power Director and

Image J software were used in data analysis.

Results: K_{IC} values were significantly higher for IPS e.max Press than IPS e.max CAD. The pilot FCP tests on Plexiglas revealed limitations with regards to the applicability of NTP specimen K_{IC} test to FCP studies due to the presence of a trapezoidal crack front in the specimens.

Conclusion: IPS e.max Press is superior to IPS e.max CAD in K_{IC}. Further research should be conducted to evaluate the feasibility of using a trapezoidal crack front in FCP studies.

Preface

This in vitro study was supervised by Dr. N. Dorin Ruse. The research committee members were Drs. N. Dorin Ruse and Caroline Nguyen, from the Faculty of Dentistry, and Dr. Tom Troczynski from the Department of Materials Engineering.

Human or animal subjects and bio-hazardous materials were not used in this study; therefore, ethical approval from the UBC Research Ethics Board was not required.

Table of Contents

List of Tables

List of Figures

Acknowledgements

I cannot express enough gratitude to my supervisor Dr. N. Dorin Ruse for his continuous support and guidance. No matter how large the obstacle I faced, he always had a solution. His knowledge and dedication were essential for the completion of this project and I thank him deeply for this wonderful learning opportunity.

Besides my supervisor, I offer my deepest appreciation to my committee members: Dr. Tom Troczynski and Dr. Caroline Nguyen for their time and efforts in providing me with their constructive feedback.

In addition, I would like to thank my sponsoring institution, King Saud bin Abdulaziz University for Health Sciences, and the government of Saudi Arabia for giving me this unique opportunity to become a specialist in my field by financially supporting my education over the course of the program.

Finally, I would like to thank Ivoclar Vivadent for supplying the materials used in this project.

Dedication

To my precious family: my mother, Hanan, my father, Tarek and little brother, Mohammad. I thank you for believing in my dream no matter how impossibly far away it seemed in the beginning. Leaving home and being physically and literally on the other side of this planet was not easy, yet your love and support (and skype) made it possible.

To my loving husband, Aziz, thank you for the nights we spent in the coffee shop working together on our projects. Thank you for the days we spent on the beach trying to forget about them. Thank you for everything else in between.

Chapter 1: Introduction

Since ancient times, teeth have been considered essential for beauty, function and speech, and therefore, humans have been creative in using materials naturally found to replace their teeth when they were lost by accident or due to disease. The earliest evidence of dental treatment goes back to 4000 BC in Egypt, the medical center of the ancient world. There, archeologists have found what is thought to be the first dental prosthesis consisting of a natural tooth replacing an extracted third molar by tying a gold wire to link it to the adjacent second molar[1]. Evidence of tooth replacements were also found from the early Greeks, Etruscans and Romans[2].

Until the 18th century, only minimal progress was achieved in prosthetic dentistry, until the work of Pierre Fauchard, who is considered the father of modern dentistry, helped make it a profession of high standards. Dentists of that time utilized naturally occurring materials to replace human teeth, including ivory, wood, stone, animal teeth or extracted human teeth[1].

In 1774, Alexis Duchateau, who was dissatisfied by discolored ivory dentures, fabricated a ceramic denture, therefore becoming the first person to use ceramics successfully in dentistry[1, 3]. In 1844, ceramic denture teeth were manufactured by S.S White and in the years that followed many manufacturers also started producing ceramic teeth in an attempt to mimic natural teeth in esthetics[1]. Ceramics became popular due to their ability to overcome many of the drawbacks of previously used materials, such as corrosion in saliva, discoloration and poor esthetics[1].

Over the years and until today, new ceramic products have been introduced to the market, each claiming to be superior to the others in esthetic and physical properties. With the introduction of computer-aided design/computer-aided manufacturing (CAD/CAM) techniques, a new category of machinable ceramics became increasingly used to fabricate restorations that could be digitally designed and milled[4].

1.1 Computer-Aided Design/ Computer-Aided Manufacturing (CAD/CAM)

With the introduction of CAD to the world of industry in the 1950s, the possibilities seemed endless and it was only a matter of time until this technology was incorporated into dentistry. In the beginning, however, the process was far from being smooth and there were many obstacles in the way of digitally designing dental restorations, including the limited computing power. Limitations were also due to CAM devices, which were too large and lacked the dimensional reproduction accuracy needed for dental purposes [5]. Despite the difficulties, dental researchers and manufacturers continued to improve this very promising area of dentistry.

In general, a CAD/CAM system consists of three main components: (1) a digitizing tool, or scanner, that transfers the numerical data to a computer; (2) a computer with appropriate software to process the digital data and design the final product to be machined; and (3) a machine that transforms the design into an object [6].

Depending on the location of these three main components, the production of dental restorations by this technology can take place either chair-side, in a dental lab, or in a production center [6].

In 1971, Dr. Duret introduced the Sopha system, which was the first CAD/CAM system in the history of dentistry. However, this system was not successful in gaining popularity, probably due to the primitive computer abilities available at that early time [7,8].

Dr. Moermann, a co-developer of the CEREC system (Sirona Dental Systems GmbH, Bensheim, Germany), was one of the pioneers in the development of the currently known dental CAD/CAM systems. The CEREC 1 system introduced in 1983, was the first to succeed in optically and three-dimensionally measuring a dental cavity using a compact intraoral camera with a laser displacement gauge connected to a computer. The design of the restoration was made on the computer and then the numerical data was transferred to a chair-side compact machine to mill inlays from a porcelain block against a grinding wheel [9]. The CEREC 2 system was a modification of the previous CEREC 1 design by the addition of a cylindrical diamond bur to enable the milling of partial and full coverage crowns. The CEREC 3 system replaced the grinding wheel with another cylindrical bur, making the machine a 2-bur system for additional milling precision. Along with the hardware development, a parallel development took place in the software used in designing digital restorations. The 2D display was substituted by a 3D display for a better representation of the prepared tooth structure on the screen and an improved restoration designing experience [9].

Another pioneer was Dr. Anderson, the developer of the Nobel Procera CAD/CAM system (Nobel Biocare, Gotenborg, Sweden). In the beginning, the system was used to produce titanium substructures that were later veneered with low fusing ceramic. Nowadays, it is also used in the production of all ceramic crowns from aluminum oxide or zirconium oxide. In this system, the

scanner with a contact probe is used to scan a final cast of the prepared teeth and then the data is transferred to a computer where the design of the restoration is finalized. The fabrication of the restoration takes place at a distant production center in Sweden [10].

From that point forward, many other systems were developed to be used chair-side or in the dental lab. In addition, multi-axis milling machines were developed for commercial production of restorations, from metallic and ceramic materials, with increased accuracy and precision. Digitizing tools were also improved and new methods of capturing the data were introduced, making CAD/CAM technology the future of dentistry [7].

The marginal and internal fit of restorations made with CAD/CAM technology was tested in several studies [7,11]. The results of these studies show that their accuracy of fit is acceptable compared to the conventional methods of fabrication.

1.2 Dental Ceramics

Ceramics is a very broad term. According to Smith, "Ceramics are crystalline, inorganic, non-metallic materials which consist of metallic and non-metallic elements bonded together primarily by ionic and/or covalent bonds" [12]. Glasses are similar to ceramics in composition and in type of bonds, but differ structurally because their composition is heated to fusion and then cooled to reach a rigid state without crystallization[12].

1.2.1 Traditional Ceramics and Engineering Ceramics

Ceramics, in general, can be categorized into two classes: traditional ceramics and engineering ceramics [12]. Raw materials of traditional ceramics are naturally found in earth. These include clay, feldspar and silica [12]. Humans, over 26,000 years ago, learned to form these raw materials into objects that were later processed, by subjecting them to high temperatures, to achieve higher strength and hardness [13]. All of these naturally occurring materials are silicates, since silicon and oxygen are the main elements in their structure. The basic building block of these materials is the silicate tetrahedron (SiO_4^{4-}). One electron per oxygen atom is available for bonding and according to the type of atom bonded to it, many different structures can be produced [12].

Clay is the name given to several earthy materials consisting of very small grains that plasticize upon hydration and solidify upon dehydration. The chemical structure of clay consists of a sheet of interconnected silicate tetrahedra. Three corner oxygen atoms of each silicate tetrahedra are shared among adjacent tetrahedra to produce a negatively charged sheet ($Si_2O_5^{2-}$), which is neutralized by combining it with a positively charged sheet of aluminum hydroxide ($Al_2(OH)_4^{2-}$), resulting in the formation of a two-layer clay mineral, such as Kaolinite[12].

Silica (SiO_2) is formed when all four oxygen atoms of silicate tetrahedra are shared between adjacent tetrahedra to form a 3D network. The three crystalline forms of silica are quartz, tridymite and cristobalite [12], each stable at different temperatures

Feldspar is formed when some AlO_3^{3-} anions replace SiO_4^{4-} anions resulting in a negative net charge due to the fact that the former has only three oxygen atoms to share while four are required to keep the structure electrically neutral. Cationic species, such as Na^+, K^+, Ca^{2+}, Mg^{2+}, Ba^{2+} , are then incorporated into the network to neutralize it[12].

Traditional ceramics lack the required mechanical properties for modern applications, which led to the introduction of engineering ceramics, such as alumina (Al_2O_3) and zirconia (ZrO_2) (as partially stabilized zirconia).

1.2.2 Ceramics in dentistry

One of the earliest uses of ceramics in dentistry was in the fabrication of complete denture prostheses by Alexis Duchateau in 1774[3]. The first successful use of ceramic systems in modern fixed prosthodontics was the use of the traditional feldspathic ceramic in the fabrication of the porcelain jacket crown by Charles Land[14]. This crown was later reinforced with alumina particles by McLean to improve its properties[15].

Due to their natural appearance, biocompatibility and optical properties, ceramic materials have been increasing in popularity ever since and manufacturers have been developing new systems to meet the demand[16]. The numerous available ceramic materials can be classified in several ways, according to their composition, processing method, firing temperature, microstructure, translucency, fracture resistance or abrasiveness and uses[17].

According to their composition, the spectrum of dental ceramics can be classified into the following categories: (1) feldspathic (glass ceramic, leucite reinforced, mica reinforced, lithium disilicate reinforced); (2) glass infiltrated alumina/ spinell/ zirconia core; (3) alumina core; (4) zirconia core [4].

Feldspathic ceramics are predominantly glass-ceramics, with an amorphous matrix derived from the natural mineral feldspar reinforced with silica. Clay does not contribute to the composition of feldspathic dental ceramics because the formability of clay is not a required feature for dental applications [12].

A subsequent advancement in the traditional feldspathic ceramic composition was the addition of various fillers to improve mechanical properties. One major improvement was achieved in 1962 when leucite (with a coefficient of thermal expansion (CTE) of 20-25 ppm/^{o}C)[18] was incorporated into the composition of feldspathic ceramic (usually with a CTE as low as 7.5 ppm/^{o}C)[18] used to veneer metallic substructures (CTE of most alloys suitable for veneering with ceramic is around 14-15 ppm/^{o}C)[19]. Leucite ($K_2O.Al_2O_3.4SiO_2$) is a potassium alumino-silicate, which crystallizes when feldspathic ceramic is reheated, leading to an increase in the CTE of the feldspathic ceramic, bringing it close to, but slightly lower (about 0.5 ppm/^{o}C lower)[20] than that of the metal substructure being veneered, therefore placing the ceramic under slight compression[3, 16]. When used for all ceramic applications, leucite reinforced glass ceramics are still considered one of the most esthetic ceramics available[16].

Despite the popularity and acceptance of metal ceramic systems, the increased demand for the superior esthetics of metal-free restorations has encouraged manufacturers to introduce new materials to be used in the fabrication of all ceramic restorations.

Vita Mark I and II (VITA Zahnfabrik, Bad Sackingen, Germany) are machinable feldspathic ceramics marketed to be used in CAD/CAM technology. IPS Empress (Ivoclar Vivadent, Schaan, Liechtenstein) is a leucite reinforced glass ceramic that is processed by melting and pressing, following the traditional lost wax technique. IPS ProCAD (Ivoclar Vivadent, Schaan, Liechtenstein) is a machinable ceramic that has a similar composition as IPS Empress but is intended to be used in CAD/CAM processing. Other fillers have been incorporated into the composition of glass ceramics, such as mica in Dicor (Densply Inc, York, PA, which was discontinued) and lithium disilicate in IPS Empress 2 (Ivoclar Vivadent, Schaan, Liechtenstein) and more recently in IPS e.max CAD and IPS e.max Press (Ivoclar Vivadent, Schaan, Liechtenstein) [4].

The desire for materials with better mechanical properties has led to the introduction of two additional strategies to strengthen ceramics. The first was to reinforce the ceramic with a continuous 3D framework formed by an industrial-type ceramic material, capable of better resisting crack propagation, and the second was to entirely eliminate the glassy matrix[21]. In-Ceram Alumina, In-Ceram Spinell and In-Ceram Zirconia (VITA Zahnfabrik, Bad Sackingen, Germany) demonstrate how the first strategy was applied. In-Ceram Alumina has been introduced as a core material for crowns and anterior 3 unit fixed dental prostheses (FDPs). This ceramic core is fabricated through the slip casting technique. In this technique, a porous

continuous 3D framework of sintered alumina particles is made, which is later infiltrated with a low viscosity feldspathic glass-ceramic during a second firing, to achieve a high esthetic result[4].

To overcome the problem of the high opacity of In-Ceram Alumina, another core material, In-Ceram Spinell (VITA Zahnfabrik, Bad Sackingen, Germany) was introduced. It contains a mixture of alumina and magnesia, which imparts a higher translucency to the material compared with In-Ceram Alumina. On the other hand, the flexural strength of this material is lower than In-Ceram Alumina [4].

More recently, In-Ceram Zirconia (VITA Zahnfabrik, Bad Sackingen, Germany) joined the In-Ceram product spectrum, with the intention of producing a stronger material that could be used to restore the posterior areas of the mouth. This was achieved by the addition of 35% of partially stabilized zirconia to the slip composition of In-Ceram Alumina [4].

Industrial pure monophase ceramics were developed by sintering the crystalline phase together without a glassy matrix in between the crystals to form a dense polycrystalline structure[3]. This process resulted in ceramic materials with superior mechanical properties but high opacity and therefore, they are best used as cores that are later veneered with feldspathic ceramic for the best esthetic result. The two materials produced by this technique are aluminum oxide (alumina, Al_2O_3) or zirconium oxide (zirconia, ZrO_2) [4].

An example of an alumina-based polycrystalline ceramic product is Procera (Nobel Biocare AB, Goteborg, Sweden). Zirconia based polycrystalline products include Lava (3M ESPE, St. Paul, Minn) and Cercon (Densply Ceramco, York, Pa).

The natural esthetic appearance of ceramics is attributed to their translucency. Moreover, compared to gold or amalgam, less plaque adheres to a smooth ceramic surface, resulting in superior hygiene and better tissue response.[17, 22] However, there are still considerable concerns regarding their mechanical properties[14]. The stiff and brittle ceramic materials may exhibit catastrophic fracture, in particular when exposed to tensile stresses[23], which remains the main cause of their failure [24].

Table 1: Mechanical properties of different ceramics according to their manufacturers' reported values

Material	Flexure strength (MPa)	Fracture toughness (MPam½)	Coefficient of thermal expansion ppm/ ^{o}C	Modulus of elasticity (GPa)
IPS e.max Ceram[25]	90 ± 10	NA	9.5 ± 0.25	60-70
IPS e.max Press[25]	400 ± 40	2.5 – 3.0	10.15 ± 0.4	95 ± 5
IPS e.max CAD[25]	360 ± 60	2.0 – 2.5	10.15 ± 0.4	95 ± 5
VITA In-Ceram Alumina[26]	500	3.9	7.4	280
VITA In-Ceram Zirconia[26]	600	4.4	7.8	258
Lava[27]	>1100	5-10	10	>205
Cercon[28]	>1300	9	10.5	210

1.3 IPS e.max

IPS e.max is the brand name given by Ivoclar Vivadent to a range of all-ceramic products that include four core materials (IPS e.max Press, IPS e.max CAD, IPS e.max ZirPress, IPS e.max ZirCAD) and a veneering material (IPS e.max Ceram). The products of interest (IPS e.max Press and IPS e.max CAD) are both lithium disilicate glass ceramics that were designed to have two different processing pathways for the fabrication of all ceramic restorations. Both materials can be used to produce cores that can be veneered with feldspathic ceramic (IPS e.max Ceram). They can also be used as monolithic materials in the fabrication of full contour restorations[25].

1.3.1 IPS e.max Press

IPS e.max Press is supplied as ingots of lithium disilicate glass ceramic available in four translucencies and two sizes. The microstructure consists of approximately 70% lithium disilicate crystals measuring 3-6 μm in length. This product is processed utilizing the lost wax technique, which involves waxing the restorations to the desired contours, spruing and investing the wax patterns, melting the wax to create a mold within the investment and then pressing the molten ceramic into the mold in a special furnace developed specifically for this product (Programat EP 3000, EP 5000). After that, the restorations are divested, polished, characterized and glazed prior to delivery[25].

1.3.2 IPS e.max CAD

IPS e.max CAD is a lithium disilicate glass ceramic designed to be used in CAD/CAM technology. A process called pressure casting leads to the production of partially crystallized IPS e.max CAD blue blocks. These blocks are composed of 40% lithium metasilicate crystals, ranging in size between 0.2 to 1.0 μm, embedded in a glassy matrix. Their partially crystallized state facilitates the milling process with minimal wear to the milling burs[25].

After milling the restorations to the desired shape and contour, they are tempered to 850 °C in a furnace developed by the manufacturer for this material (Programat 300, 500). In this process, lithium metasilicate crystals are transformed into lithium disilicate crystals (70 % volume fraction), which are responsible for the material's high strength. The coloring ions responsible for the blue color in the partially crystallized stage also show a different oxidation state when tempered, leading to the desired tooth color and opacity[25].

1.3.3 Clinical performance of IPS e.max

Clinical evidence shows that IPS e.max Press has a survival rate of approximately 96.6% in 3 years for single crown restorations[29]. A study that evaluated fixed dental prostheses (FDPs) fabricated from monolithic IPS e.max Press and observed for a mean period of 121 months found the survival rate to be 100% after 5 years and 87.9% after 10 years. The success rate was 91.1% after five years and 69.8% after 10 years[30]. A clinical evaluation of single IPS e.max CAD

crowns showed 100% success after 2 years[31]. There is a lack of long or short term controlled clinical trials comparing IPS e.max CAD and IPS e.max Press.

1.4 Fracture Mechanics

Although fractures have been a problem for as long as man-made structures have existed, fracture mechanics is relatively young as a science. Following World War II, when Liberty ships (EC-2) fractured in half [32], people became more aware and interested in fracture mechanics. The ships, which were made from carbon steel, became brittle when exposed to lower temperatures in the Atlantic Ocean, which led the steel to undergo a ductile to brittle transition and fracture[32]. Because the consequences of such drastic fractures were detrimental to humans' lives, the discipline of fracture mechanics began to flourish. It was soon realized that understanding fracture mechanics could lead to better materials selection and could help design structures and new materials able to resist fractures where fabrication defects and cracks are difficult/impossible to avoid [32].

1.4.1 Fracture Toughness (K_{IC})

Fracture toughness is an intrinsic material property used to characterize dental materials in vitro. It describes the material's ability to withstand unstable crack propagation [33].

When a crack exists in a structure, stresses are concentrated at the crack tip upon loading and the stress intensity created by this situation is designated by "K". When the load is tensile and

creates a purely straight opening of the crack, it is termed "mode I". When the stress reaches a critical point designated by "C", the crack becomes unstable and quickly propagates to lead to the catastrophic fracture that separates the structure into two pieces. Thus, fracture toughness (K_{IC}) represents the critical stress intensities for mode one opening and is used to characterize materials regardless of the size of the crack[22].

To ensure reproducibility, international standardization of the testing procedure has been accomplished through detailed description of specimen configuration and dimensions as well as tests protocols[34]. There are several commonly used configurations in dental materials testing. One of the most common ones is the chevron-notched short rod (CNSR) specimen[34]. However, preparing a sample to be tested according to the specifications of this test's specimen could be cumbersome and, therefore, a new testing method has been developed to overcome these difficulties, which is called the notchless triangular prism (NTP) specimen K_{IC} test. [35]

1.4.1.1 The Notchless Triangular Prism specimen K_{IC} Test

As mentioned earlier, one of the common methods to test fracture toughness is to utilize the CNSR specimen configuration developed by Barker[36]. To prepare a specimen of this configuration, a chevron notch is cut into a cylindrical specimen. This process can be difficult to achieve, particularly with brittle materials such as ceramics[35].

In order to overcome the difficulties associated with specimen preparation in the CNSR method, the NTP specimen was developed[35]. The NTP specimen (Figure 1) measures 6x6x6x12 mm and,

when fitted into the specifically designed holder, achieves a final configuration similar to that of the CNSR specimen, therefore, eliminating the difficult notching procedure [35]. The specimen holder (Figure 2) consists of 4 parts: two symmetrical half cylinders, with a loading collar at one end and a triangular prismatic groove at the other end from the base; two symmetrical half disks fastened with screws across the triangular prismatic grooves of the corresponding half cylinders restrain the specimen. To mount a specimen, a special mounting block consisting of two halves is used. The two halves slide horizontally, which allows a 20 – 500 μm spacer to fit in between the two halves of the holder. A ~0.1 mm deep crack is initiated into the triangular prism specimen at a point midway along one of its edges. This crack is aligned with the split line created by the spacer between the two halves of the holder. The screws are then tightened on the holder to hold the specimen in place [35]. The specimen can then be used for fracture mechanics testing, specifically K_{IC}.

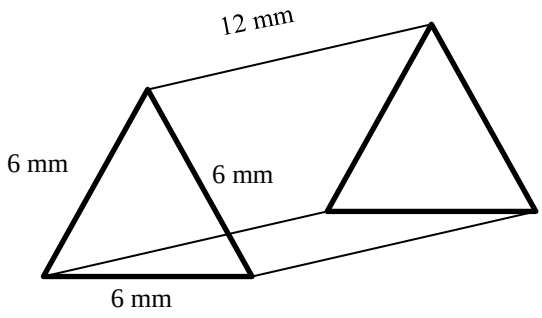

Figure 1: NTP specimen

Figure 2: NTP specimen holder

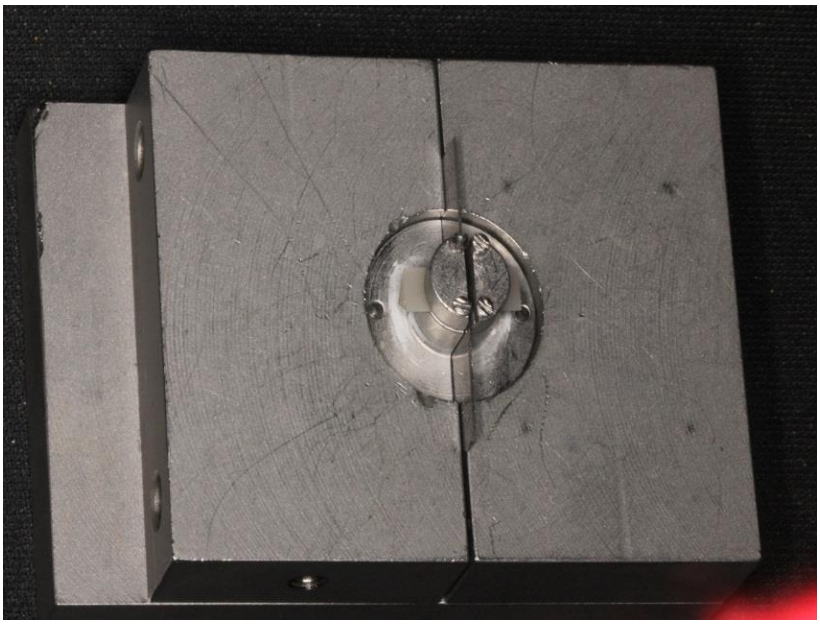

Figure 3: NTP specimen holder in mounting block with metal spacer

After its introduction, this test was validated through finite element analysis. In addition, a calibration study was done in which materials of known K_{IC} were tested using the NTP and the CNSR methodologies and comparable results were obtained [35]. It was determined that NTP was

a suitable testing methodology for materials as well as adhesive interfaces [35]. Several investigators have utilized this testing modality in mechanical characterization of dental tissues and materials [37-40].

1.4.2 Fatigue Crack Propagation

When a crack, of length $\boldsymbol{a}$ and crack tip curvature $\boldsymbol{\rho}$ exists in a structure, the stress at the crack tip ($\boldsymbol{\sigma_{max}}$) is significantly increased relative to the stress applied ($\boldsymbol{\sigma_a}$) (see equation below), which leads to a decreased strength[22].

$$\sigma_{max} = 2\sigma_a \sqrt{\frac{a}{\rho}}$$

However, it is rare for a critically large crack to exist initially; rather, a smaller crack propagates under cyclic loading, eventually leading to catastrophic failure of the structure under stresses considerably lower than its strength[34], a process called fatigue. For this reason, the determination of the fatigue crack propagation (FCP) parameters in addition to K_{IC} is an essential part of the fracture mechanics design approach[41].

Until recently, the vast majority of published literature about fatigue related to metal fatigue[42,43]. As this type of testing was adopted in dentistry, testing FCP of dentin was done by several investigators[44-46]. Lately, there has been an increasing interest in the fatigue testing of high strength, brittle materials, such as ceramics[47, 48].

In a typical fatigue test, the specimen is pre-cracked and crack propagation is achieved by cyclic loading of the specimen. Crack length is measured, as a function of elapsed fatigue cycles, either visually, using a low-power microscope, or by an equivalent method, such as monitoring changes in the stiffness of the specimen, changes in the voltage field, or monitoring ultrasonic waves that are reflected off the crack[33].

Numerical analysis of the data is done to calculate fatigue crack growth rate, da/dN. Subsequently, da/dN is expressed as a function of stress intensity factor range, ΔK, obtaining a relationship that is called Paris Law[33, 49].

Paris law is used to describe the crack growth behavior of a certain material. Test data are plotted into a curve represented in Figure 4.[33]

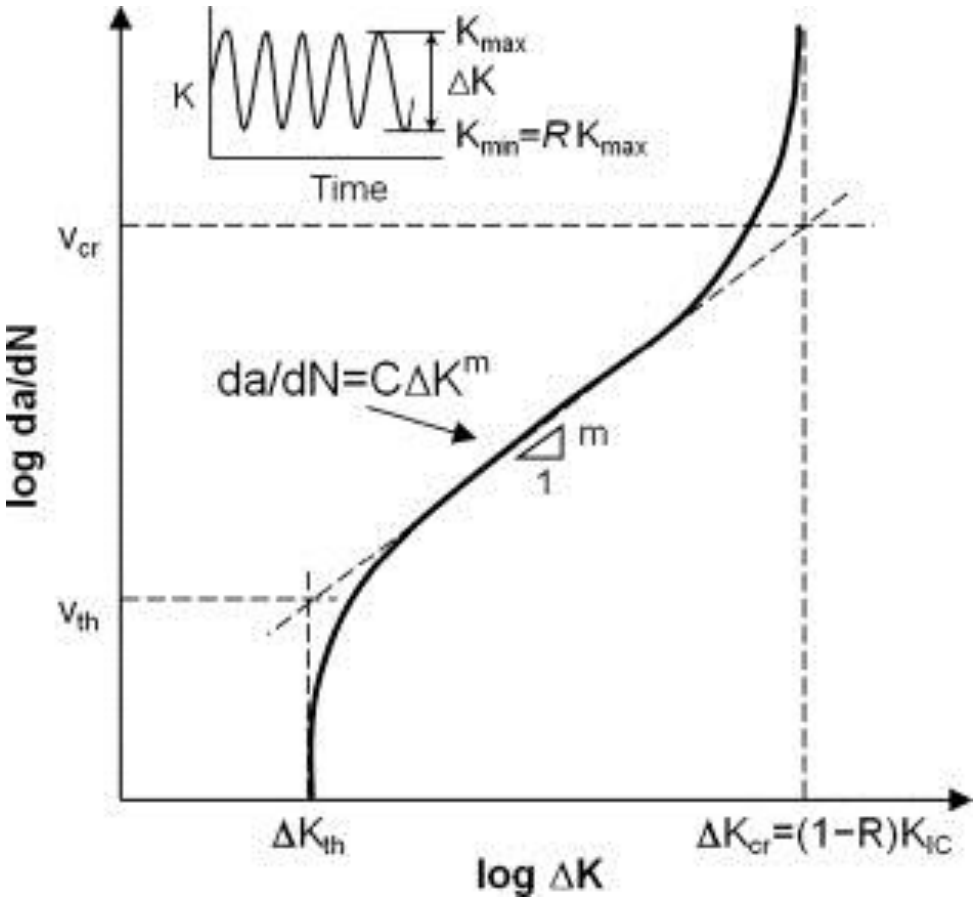

Figure 4: A typical Paris curve[50]

A typical curve consists of three main segments. The middle segment is often a straight line with a relationship represented by the following equation.

$$\frac{da}{dN} = C\,(\Delta K)^m$$

This equation was found by P.C Paris in the 1960s and has influenced the application of fracture mechanics in FCP determination ever since[33].

Below ΔK_{th}, called the fatigue crack growth threshold, crack growth does not normally happen. When the crack growth rate is high, a steep portion of the curve appears, which represents unstable crack growth prior to catastrophic failure of the specimen[33].

Temperature and hostile environmental factors can affect the results of fatigue testing[49] and this is to be taken into consideration when applying test results to clinical reality.

Chapter 2: Research Protocol

2.1 Purpose

IPS e.max Press and IPS e.max CAD are marketed by the manufacturer as clinically identical materials indicated for the same clinical uses. However, as mentioned earlier, different crystal sizes of lithium disilicate are formed during the manufacturing/processing of each of these materials. In addition, different processing methods are involved in producing a dental restoration from each material. Both of these factors could lead to significantly different mechanical properties.

It would therefore be of interest from both a materials science point of view and a clinical usage point of view to characterize the materials in the lab as a first step towards arriving to some clinical implications regarding whether one should be used over the other in any given clinical scenario.

Because K_{IC} is an intrinsic material property that correlates to clinical performance (fracture and wear), its determination could be useful in comparing IPS e.max CAD and IPS e.max Press. Moreover, since IPS e.max CAD and IPS e.max Press fail clinically under cyclic loads rather than a static load, it would be valuable to also compare their FCP parameters. Therefore, the purpose of the current study was to determine K_{IC} and FCP parameters of IPS e.max Press and IPS e.max CAD.

2.2 Hypothesis

There is no significant difference between IPS e.max CAD and IPS e.max Press with regards to their fracture toughness (K_{IC}) and fatigue crack propagation (FCP) parameters.

Ho = There is no difference between IPS e.max CAD and Press in K_{IC} and FCP parameters.

Ha = There is a difference between IPS e.max CAD and Press in K_{IC} and FCP parameters.

2.3 Expectations

While the two forms of IPS e.max are essentially lithium disilicate glass ceramic produced by the same manufacturer, the different methods of preparation and processing may lead to statistically significant differences in their mechanical properties. The larger crystals in IPS e.max Press and the Pressing procedure that requires complete melting of the ceramic ingot may give IPS e.max Press an advantage over IPS e.max CAD with regards to the measured properties (K_{IC} and FCP parameters).

Due to the brittle nature of ceramics, it is expected that the FCP test would be challenging. The difficulty would be to capture the crack propagation phase before it progresses into a catastrophic fracture.

2.4 Materials and Methods

2.4.1 Sample Size Determination

A power analysis was used to calculate the sample size (n) needed for K_{IC} test with α = 0.05, power of 80% and a standard difference (Δ) of 0.4

We used Lehr's basic formula to obtain n:

$$n = \frac{16}{\Delta^2}$$

where

$$\Delta = \frac{\delta}{\sigma}$$

Where δ is the target difference and σ is the standard deviation. Thus, in order to be able to detect a difference of 20 % between the groups, using the mean and standard deviation of a pilot sample (mean = 2 MPa·$m^{1/2}$ and δ=0.3), with α = 0.05 and a power of 80 %, n was calculated to be 9.

For materials susceptible to brittle fractures such as ceramics, Weibull statistics are recommended. In Weibull statistical analysis, the probability of failure $\mathbf{P_f}$ is related to the fracture stress (σ) by the following exponential relationship[51]:

$$P_f = 1 - \exp\left[-\left(\frac{\sigma - \sigma_\mu}{\sigma_\theta}\right)^m\right]$$

However, in order to enable analysis of the results by Weibull statistics, at least 20 samples are necessary[52]. Therefore, 20 samples of IPS e.max CAD and 20 samples of IPS e.max Press were prepared.

2.4.2 Fabrication of IPS e.max CAD Triangular Prisms

IPS e.max CAD blocks were supplied by the manufacturer (Ivoclar Vivadent, Amherst, NY). Twenty 6x6x6x12 mm NTP test specimens were prepared by cutting and grinding commercially obtained IPS e.max CAD blocks. Each IPS e.max block was mounted, using sticky wax (Kerr, Italia, Srl), to be cut into equal rectangular blocks using diamond impregnated slicing wheels (UKAM, Valencia, CA) mounted on an Isomet low speed saw (Buehler, Lake Bluff, IL), under continuous water irrigation.

Each of these smaller blocks was then ground, using a custom built holder (Figure 5) on SiC paper discs (Buehler, Lake Bluff, IL) mounted on a grinding machine (Buehler, Lake Bluff, IL) until a perfect (6x6x6x12) mm NTP was produced (Figure 6). Consecutively finer grit SiC paper, up to 600 grit, was used to polish the prisms. The prisms were fully crystalized in the Programat furnace (Ivoclar Vivadent, Amherst, NY) at 840°C (1544°F) for 20 minutes, following manufacturer's recommended protocol (Figure 7).

Figure 5: NTP specimen holder

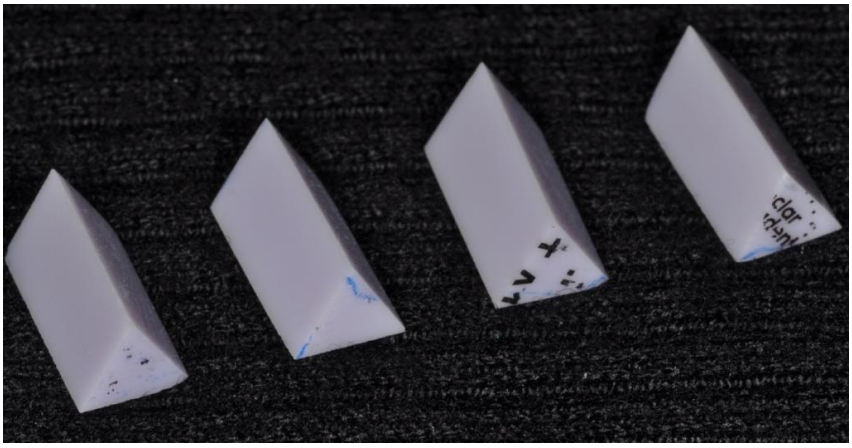

Figure 6: NTP specimens of IPS e.max CAD in the partially crystallized stage

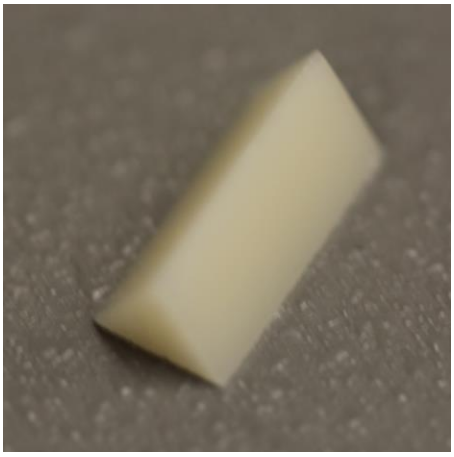

Figure 7: Crystallized IPS e.max CAD NTP specimen

2.4.3 Fabrication of IPS e.max Press Triangular Prisms

IPS e.max Press ingots were supplied by the manufacturer (Ivoclar Vivadent, Amherst, NY). Twenty 6x6x6x12 mm NTP test specimens were prepared by waxing, investing, and pressing them in IPS e.max Press. To create these wax prisms, a 6x6x6x12 mm plexiglass prism was impressed using Aquasil (Dentsply, York, PA) medium body polyvinylsiloxane impression material (Figure 8). The prism was then retrieved, leaving a mold into which melted dipping wax (Whip Mix, Louisville, KY) was poured to produce 6x6x6x12 mm wax prisms (Figure 9).

Figure 8: PVS impression of plexiglass NTP

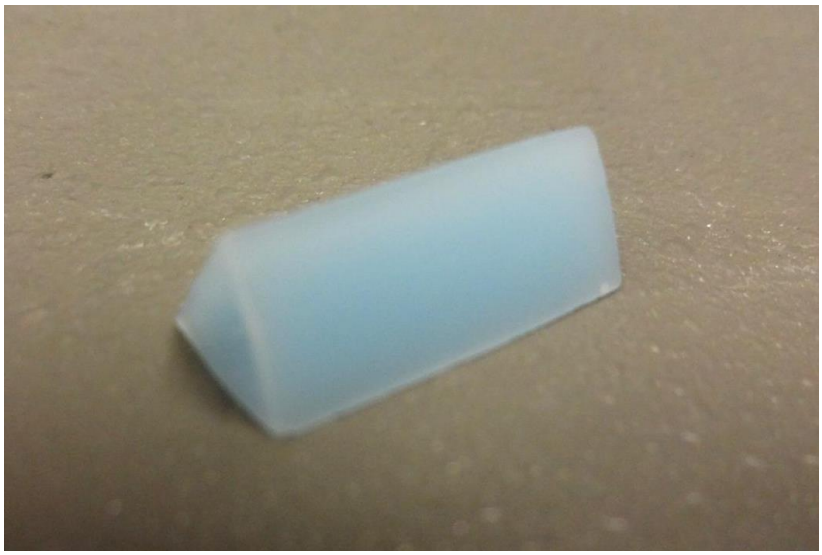

Figure 9: Wax NTP specimen

Utilizing the lost wax technique, these wax prisms were invested and IPS e.max Press was pressed into the molds (Figure 10). This pressing process was done at the Ivoclar Vivadent headquarters in Amherst, NY. The prisms were then polished to final dimensions using 600 SiC paper.

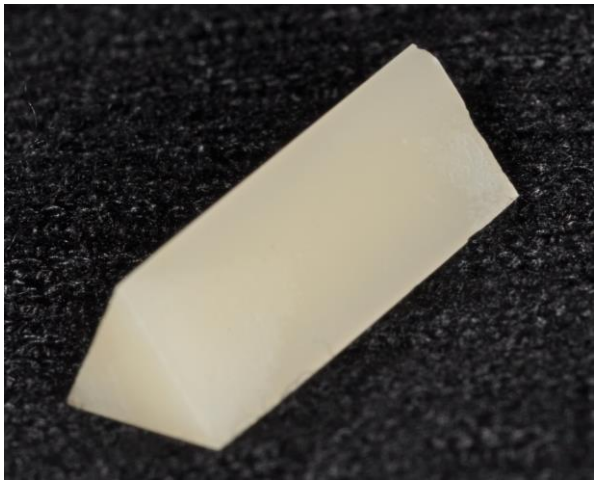

Figure 10: IPS e.max Press specimen

2.4.4 Testing Procedure

2.4.4.1 Testing K_{IC}

For determining K_{IC}, 20 (6x6x6x12) mm NTP test specimens of each material were tested. In each specimen, a pre-crack was initiated using a sharp surgical blade mounted on a wooden block. Each specimen was then mounted in the specimen holder in the fashion described in the previous NTP section of this thesis. Custom designed grips (figure 11) were used to attach the holder to a computerized universal testing machine (Instron model 4301, Instron Canada, Inc) with a 1kN Instron load cell of and an accuracy of 0.25 % of the indicated load, the assembly was loaded in tension at a crosshead speed of 0.1mm/min, and the load and displacement were monitored and recorded [35].

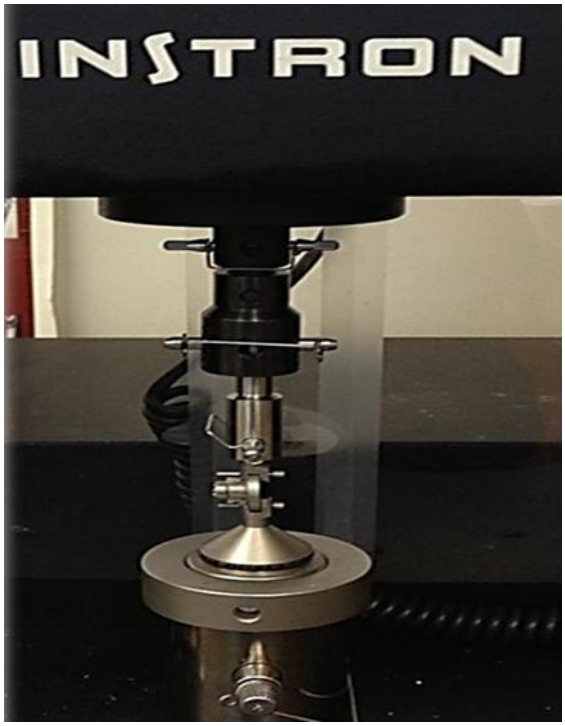

Figure 11: Custom grips attaching NTP specimen holder to testing machine

Fracture toughness was then obtained by utilizing the following equation:

$$K_{IC} = \frac{Pmax}{DW1/2} Y^*_{min}$$

Where P_{max} = maximum load recorded during testing, D= specimen diameter (12 mm), W= specimen length (10.5 mm) and Y^*_{min} = the dimensionless stress intensity factor coefficient minimum [35]. The value for Y^*_{min} is 28, as proposed by Ruse et al [27.] Fractured surfaces were characterized using scanning electron microscopy (SEM).

2.4.4.1.1 Scanning Electron Microscopy

Selected K_{IC} fractured specimens were gold coated and characterized using a Hitachi, S-3000N (Hitachi, Japan) scanning electron microscope (SEM).

2.4.4.2 Testing FCP

Because FCP testing using the NTP specimen K_{IC} test methodology had not been previously used, a pilot test was done with plexiglass NTP samples. Plexiglass NTP specimens, 6x6x6x12 mm, were obtained by grinding precut blocks, as described previously for IPS e.max CAD samples. A pre-crack was initiated in one of the specimen edges using a sharp surgical blade. Several lines, 1 mm apart were scribed on the side of the specimen to facilitate monitoring crack propagation. To scribe these lines, a putty mold that contained an impression of a triangular prism was used. The prism was placed in its impression in the putty mold and a metal ruler with grooves 1 mm apart was placed on top of the prism (Figure 12). A fresh surgical blade was used to scribe the lines through the grooves (Figure 13).

Figure 12: A putty mold and metal ruler used to scribe lines on one side of the NTP specimen

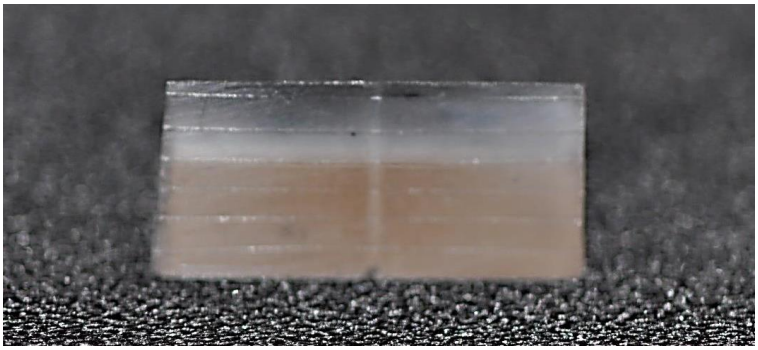

Figure 13: Lines scribed on the NTP specimen

The specimen was then secured in the NTP holder, in the same manner described previously for K_{IC} testing. The holder was then mounted on specifically designed grips (according to ASTM E647 specifications) attached to a servo hydraulic fatigue-testing machine (Instron model 8511, Instron Canada Inc).

The grips are designed with ledges that accommodate the knife edges of a strain gauge (Figures 14 and 15).

Figure 14: The grips used to attach the NTP holder and the strain gauge for testing FCP

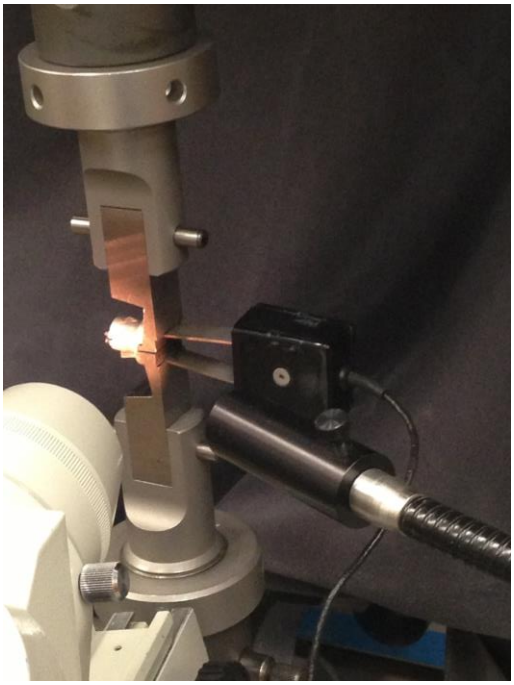

Figure 15: NTP holder attached to grips and illuminated

The specimen was cyclically loaded in tension (Mode I) in a load range between 1 N (P_{min}) and 20 N (P_{max}) ($R = P_{min}/P_{max} = 0.05$) and crack length on the scribed side of the prism was monitored and filmed using a high definition video recorder (SONY HDR-XR550V) attached to a microscope (Edmund Scientific Co, Barrington, NJ). Crack illumination was achieved by two white beam lights focused on the specimen.

The crack propagation was associated with an increase in compliance (deformation at crack tip as a function of load) and video recording was terminated once catastrophic fracture of the specimen occurred. Figures 16, 17 and 18 below are snapshots acquired from one of the video clips to illustrate the propagation of the crack.

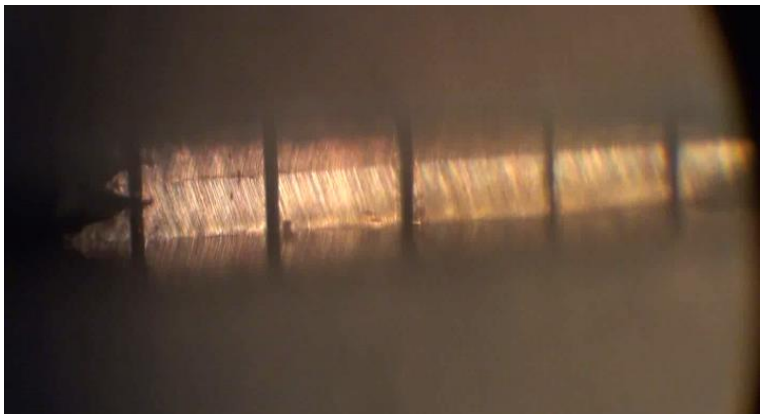

Figure 16: Initial pre-crack in an NTP specimen under cyclic loading

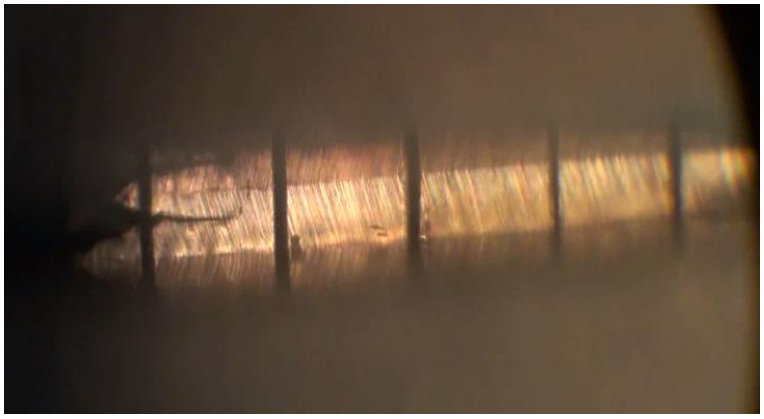

Figure 17: Crack propagation in an NTP specimen under cyclic loading

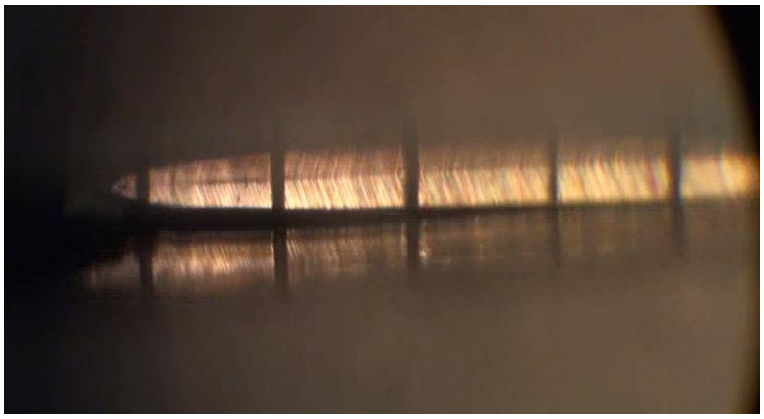

Figure 18: The last recorded crack propagation prior to catastrophic fracture

Over specific intervals of fatigue loading and until complete specimen fracture, snapshots of the video clip were obtained using Cyberlink Power Director, a commercially available video editing software (Figure 19). Image J software was used to calibrate these snapshots to the known distance between each 2 scribed lines (1 mm) and then used to measure the crack length (a) (Figures 20 and 21). These measurements were used to calculate the change in crack length (Δa) between the investigated frames.

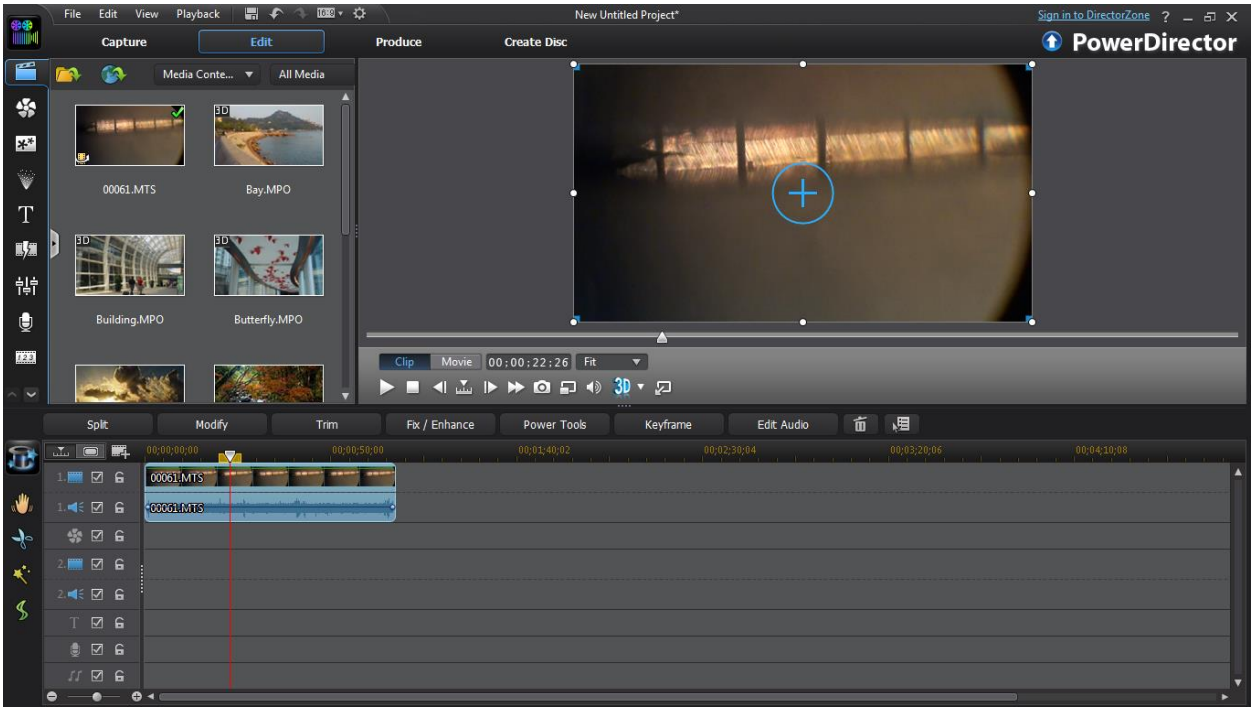

Figure 19: Cyberlink Power Director software used to obtain snapshots from FCP video clip at certain intervals

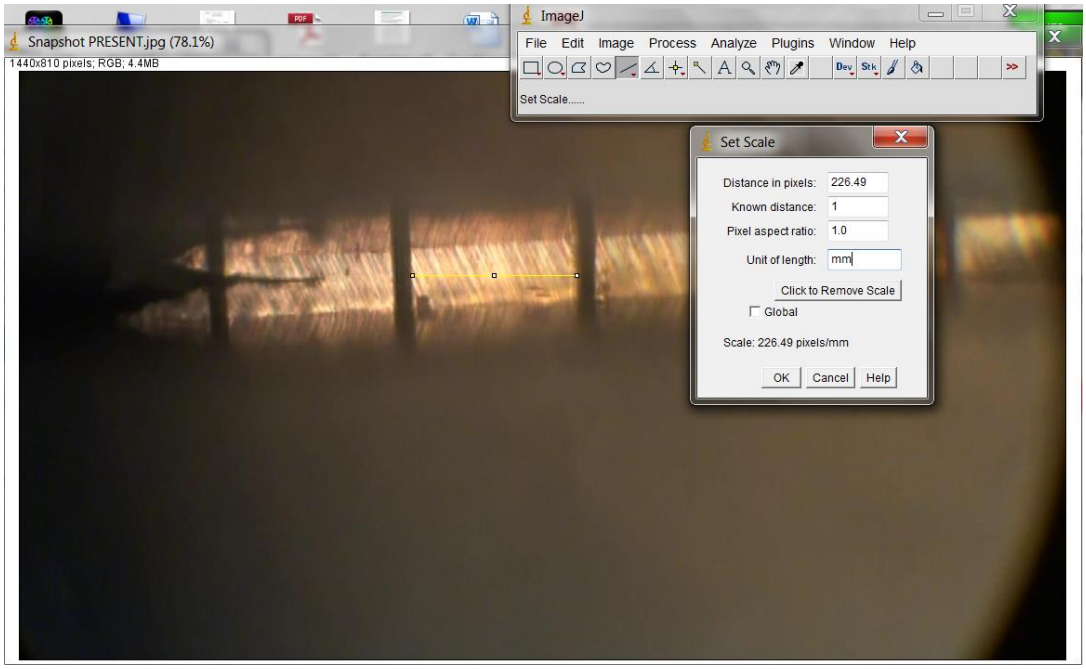

Figure 20: Calibration of measurements using Image J software

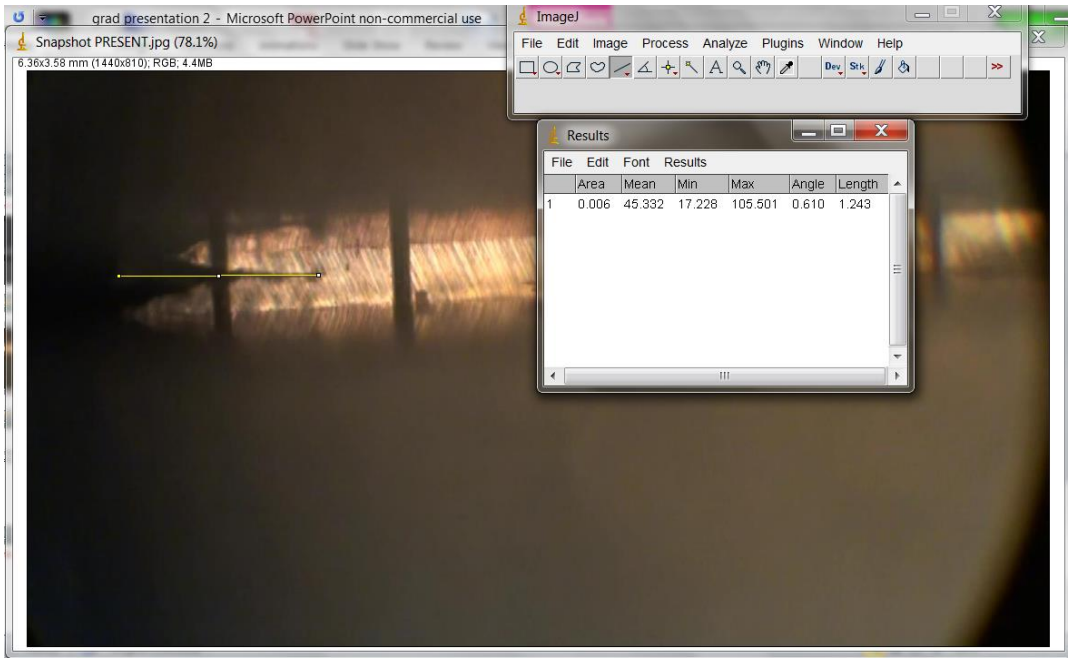

Figure 21: Measuring the crack using Image J software after calibration

The number of cycles between the assessed snapshots (ΔN) was determined based on the time at which the snapshot was taken (directly related to the number of cycles). The change in crack length vs number of cycles was plotted and the results were used to determine the fatigue crack growth rate (da/dN). A final curve of $\frac{da}{dN}$ versus ΔK was plotted on log/log scales and used to calculate FCP parameters, based on Paris' Law

$$\frac{da}{dN} = C\,(\Delta K)^m \text{ or } \log(da/dN) = m\log(\Delta K) + \log C$$

Where ΔK is the stress intensity range, C (the intercept) is the fatigue crack growth coefficient and m (the slope) is the fatigue crack growth exponent.

2.4.5 Statistical Analysis

For K_{IC}, Weibull statistical analysis was used to evaluate the characteristic strength and the reliability of each material[51]. An independent student t-test was also performed to compare the results.

2.5 Results

2.5.1 K_{IC} results

Weibull modulus, represented by the slope of the curves (Figure 22) gives an indication of the reliability of each material. The steeper the curve, the more reliable the material is. Characteristic Weibull K_{IC} is obtained from the plot at 63.2 percentile point.

As seen in table 2 and in the Weibull plot in Figure 22, the results of the K_{IC} test revealed that IPS e.max Press had higher values of both Weibull modulus **m** and characteristic Weibull K_{IC} than IPS e.max CAD. A t-test showed that IPS e.max Press had a significantly higher K_{IC} than IPS e.max CAD ($p < 0.05$).

Material	K_{IC} (in MPa·$m^{1/2}$)	Weibull modulus ɱ	Characteristic Weibull K_{IC} (in MPa·$m^{1/2}$)
IPS e.max CAD	1.79 ± 0.26a	8.41	1.90
IPS e.max Press	2.50 ± 0.31b	9.74	2.64

Table 2: K_{IC} of IPS e.max CAD and IPS e.max Press

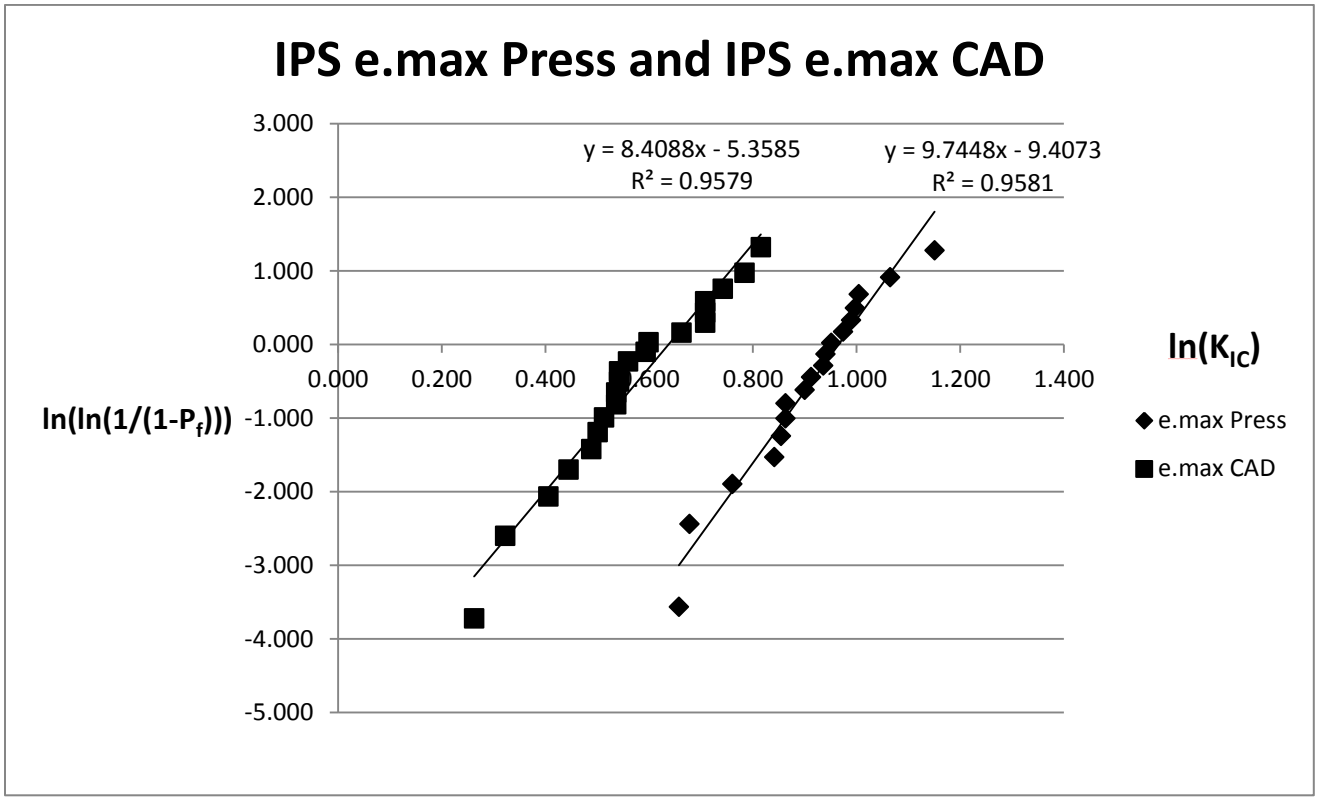

Figure 22: Weibull plot of K_{IC} results

2.5.1.1 SEM images of IPS e.max

Figures 23 to 28 present characteristic SEM micrographs of fractured K_{IC} specimens. Figure 23 (A,B) shows two halves of a fractured IPS e.max CAD prism with an arrow pointing at the initiation area. In examining the fractured surfaces at higher magnification, Figures 24 and 25 (A,B), they look smooth, possibly indicating a crack propagation through the glassy matrix.

Figure 26 (A,B) shows two halves of a fractured IPS e.max Press prism. At higher magnification, shown in Figures 27 and 28 (A,B), rough and irregular fractured surfaces are seen with minimal glassy matrix visible in the micrographs and almost entirely crystallized surfaces.

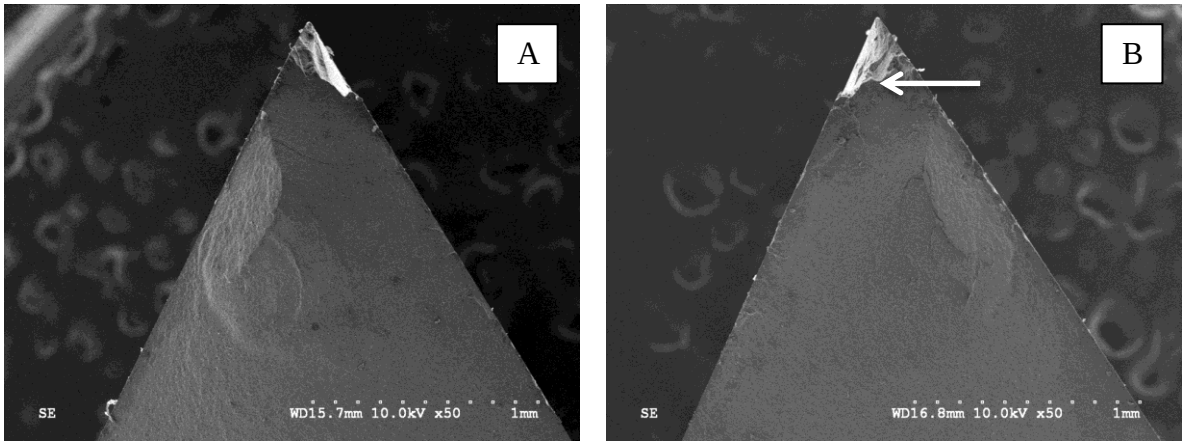

Figure 23: SEM photo of 2 sides of IPS e.max CAD prism x50 magnification

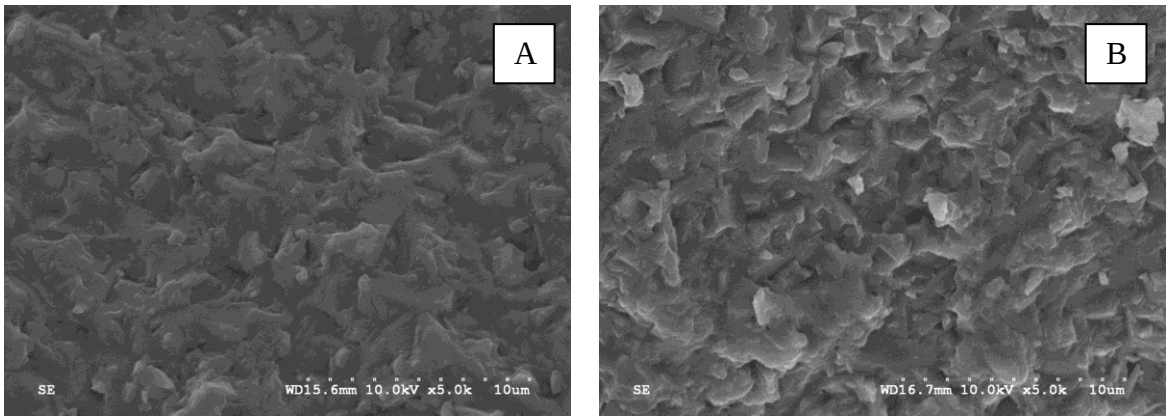

Figure 24: SEM photo of 2 sides of IPS e.max CAD prism x5000 magnification

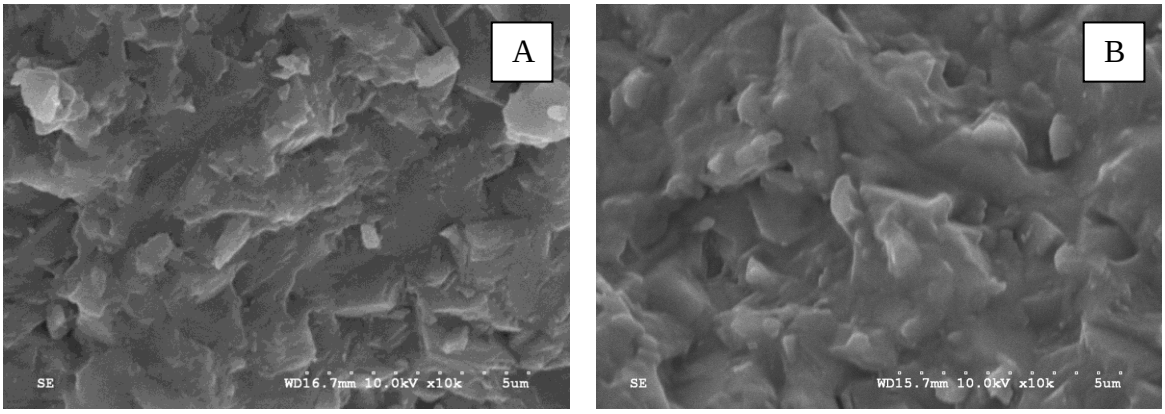

Figure 25: SEM photo of 2 sides of IPS e.max CAD prism x10000 magnification

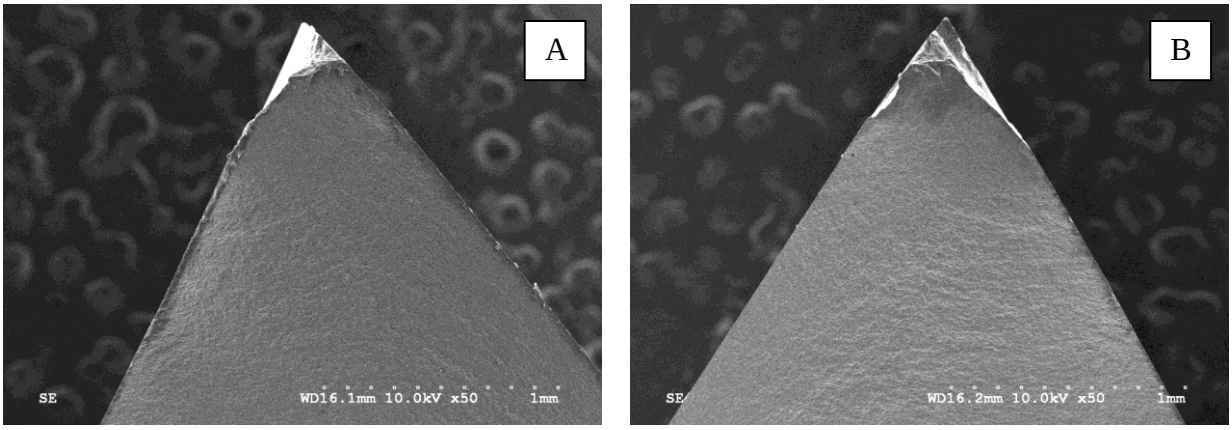

Figure 26: SEM photo of 2 sides of IPS e.max Press prism x50 magnification

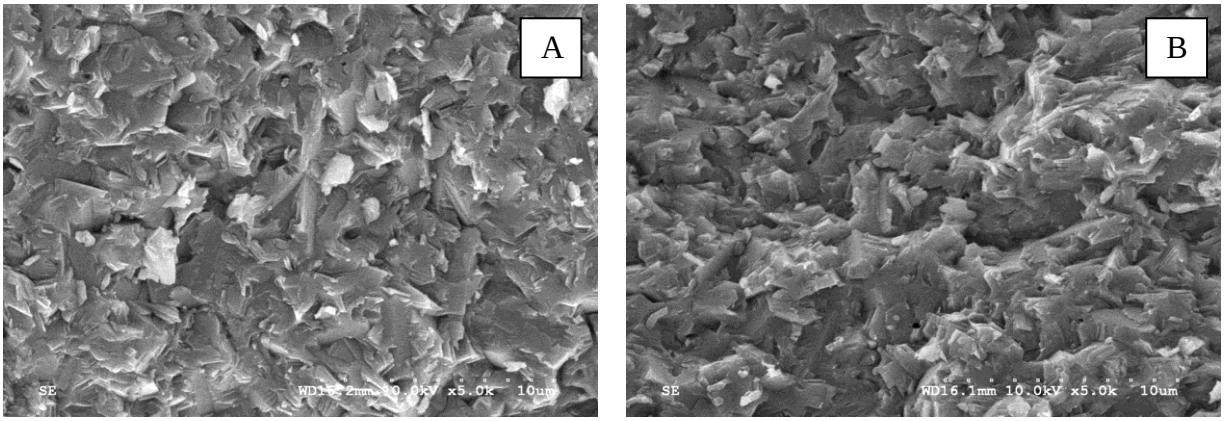

Figure 27: SEM photo of 2 sides of IPS e.max Press x5000 magnification

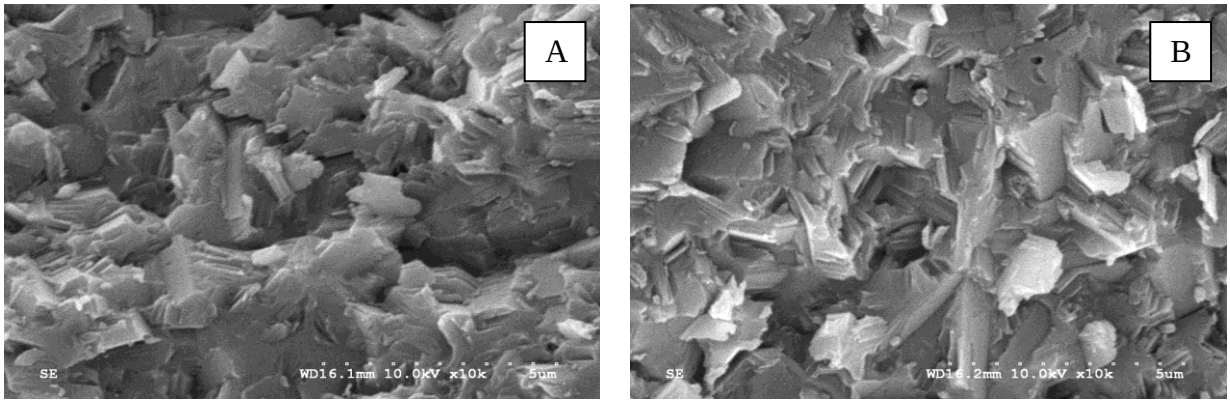

Figure 28: SEM photo of 2 sides of IPS e.max Press x10000 magnification

2.5.2 FCP results

Three plexiglass specimens were tested in the manner previously described. The following tables and graphs summarize the data obtained from these three experiments.

# of cycles (N)	a (mm)	a versus N graph
00	0.00562	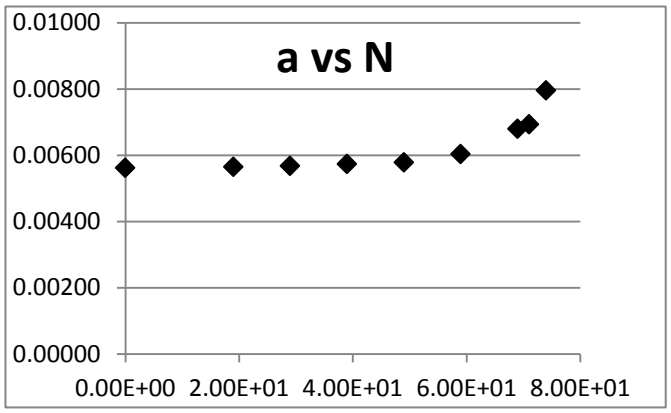
19	0.00565	
29	0.00567	
39	0.00573	
49	0.00578	
59	0.00603	
69	0.00680	
71	0.00693	
74	0.00796	

Table 3: First Plexiglass specimen (a vs N graph)

# of cycles (N)	a (mm)	a versus N graph
2	0.00575	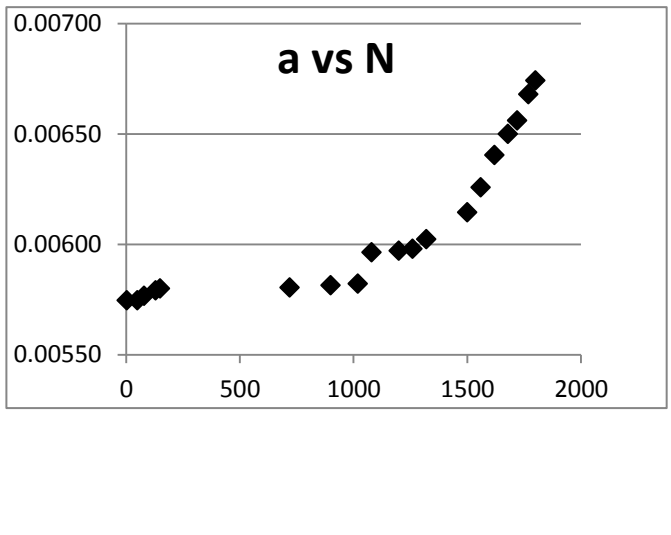
49	0.00575	
79	0.00577	
129	0.00579	
149	0.00580	
719	0.00580	
899	0.00581	
1019	0.00582	
1079	0.00596	
1199	0.00597	
1259	0.00598	
1319	0.00602	
1499	0.00614	
1559	0.00626	
1619	0.00640	
1679	0.00650	
1719	0.00656	
1769	0.00668	
1799	0.00674	

Table 4: Second Plexiglass specimen (a vs N graph)

# of cycles (N)	a (mm)	a versus N graph
0	0.00574	
41	0.00575	
80	0.00577	
130	0.00579	
150	0.00580	
320	0.00580	
360	0.00580	
420	0.00580	
480	0.00580	
540	0.00580	
600	0.00580	
720	0.00580	
900	0.00581	
1020	0.00582	
1080	0.00586	
1140	0.00586	
1200	0.00588	
1260	0.00596	
1320	0.00597	
1410	0.00598	
1500	0.00602	
1560	0.00604	
1620	0.00614	
1680	0.00626	
1720	0.00640	
1770	0.00650	
1800	0.00656	
1830	0.00668	
1878	0.00676	
1894	0.00685	
1910	0.00707	
1920	0.00710	
1936	0.00716	
1940	0.00733	
1942	0.00738	
1945	0.00748	
1948	0.00756	
1949	0.00767	

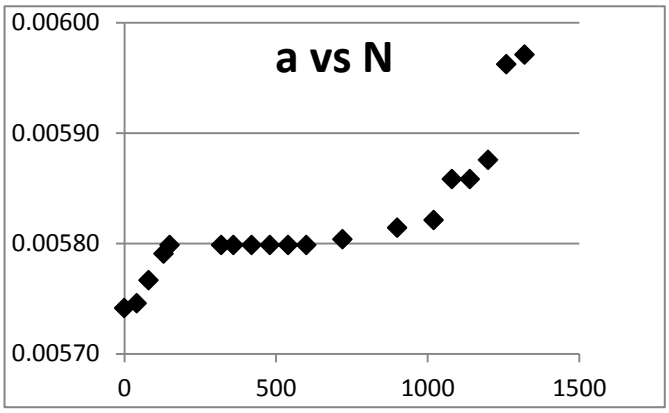

Table 5: Third Plexiglass specimen (a vs N graph)

In the attempt to calculate Y* and subsequently K_I, we found that their values did not follow the expected gradual increase with increasing number of cycles. Rather, the values fluctuated between increasing and decreasing, and the resulting graph did not follow Paris law graph.

Chapter 3: Discussion

3.1 K_{IC}

The results of the K_{IC} test showed that IPS e.max Press had higher values of both Weibull modulus **m** and characteristic Weibull K_{IC} than IPS e.max CAD. The values for Weibull K_{IC} for IPS e.max Press and CAD were 2.64 and 1.90, respectively.

These results are in agreement with the manufacturer's in-house testing reported values which are 2.5-3 for IPS e.max Press and 2.0-2.5 for IPS e.max CAD. There were no studies found comparing K_{IC} of both materials in vitro. In addition, there were no studies reporting on the individual K_{IC} values of either material.

Several studies were found reporting on K_{IC} of IPS Empress 2, which is IPS e.max Press's predecessor. IPS Empress 2 is also a lithium disilicate pressable glass ceramic manufactured by Ivoclar Vivadent. The results of these studies for K_{IC} of IPS Empress 2 were 3.4[53] and 3.14[54].

The difference we found between K_{IC} values for IPS e.max CAD and Press can be attributed to the difference in crystals size reported by the manufacturer. When examining the SEM images (Figure 29), IPS e.max Press appears to have a rougher surface, almost entirely crystalized with minimal glassy matrix. On the other hand, IPS e.max CAD had a smooth surface and the crack seemed to propagate within the glassy matrix. This could mean that more energy was needed to

penetrate the rougher, more irregular IPS e.max Press surface than what was needed for IPS e.max CAD.

In addition, it may be necessary to revise the crystallization cycle recommended by the manufacturer for IPS e.max CAD, as the fractured surfaces did not appear to be fully crystallized when examined under SEM.

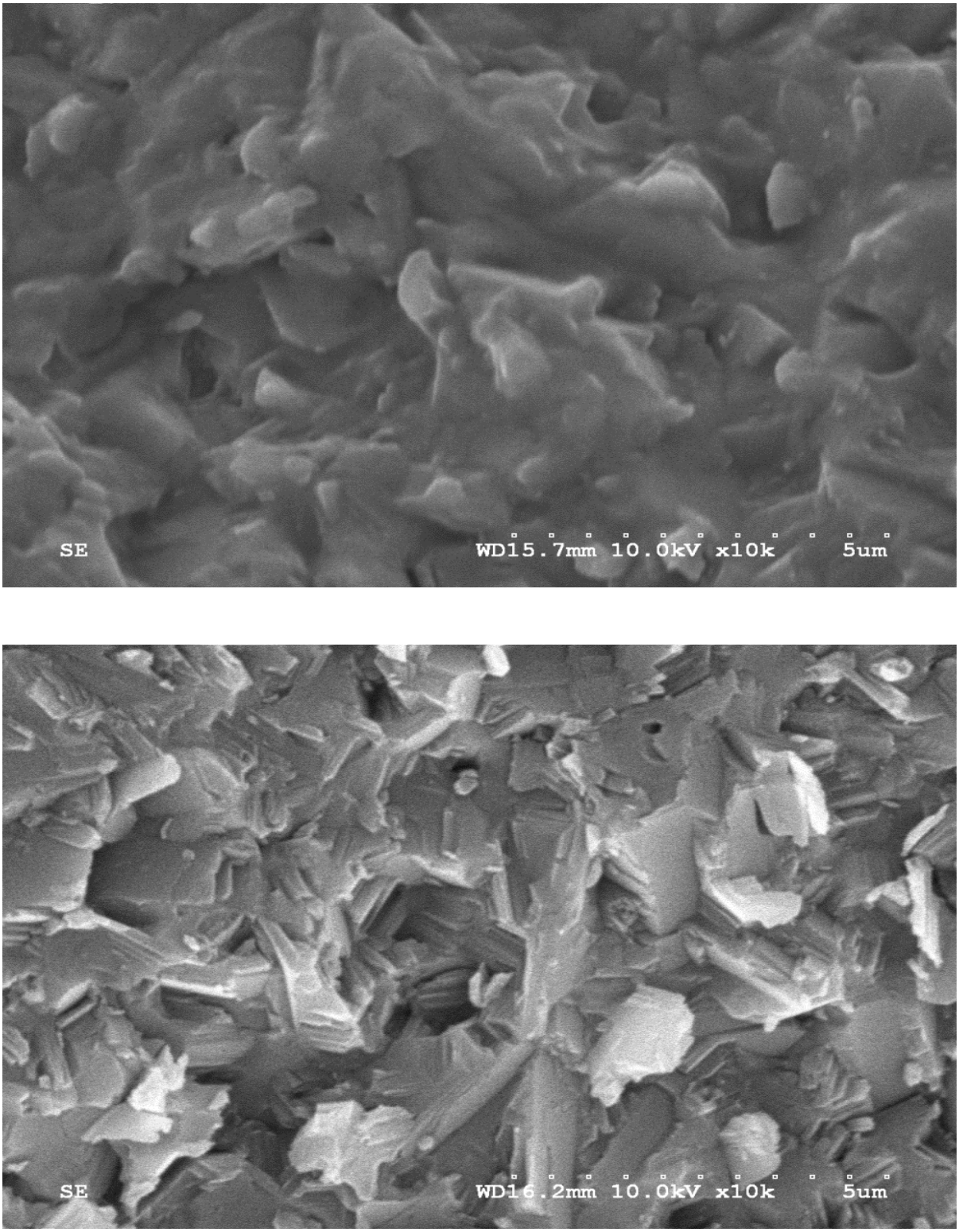

Figure 29: SEM photos comparing IPS e.max CAD (above) and IPS e.max Press (below) x10000 magnification

3.2 FCP

The results we got from this test varied from what was expected, as Y^* and K_I values were not gradually increasing as one would expect with increasing number of cycles.

To explain these results, we compared the NTP specimen to the compact tension specimen commonly used in FCP tests. Unlike a compact tension specimen, where the crack front (b) progresses in a constant width, in the short rod chevron notch (SRCN) specimen, and consequently in the notchless triangular prism (NTP) specimen, **b** is trapezoidal, which implies a constant crack front increase with crack growth. The crack front is calculated using the following equation: $b = D\ \frac{a1-ao}{a-ao}$

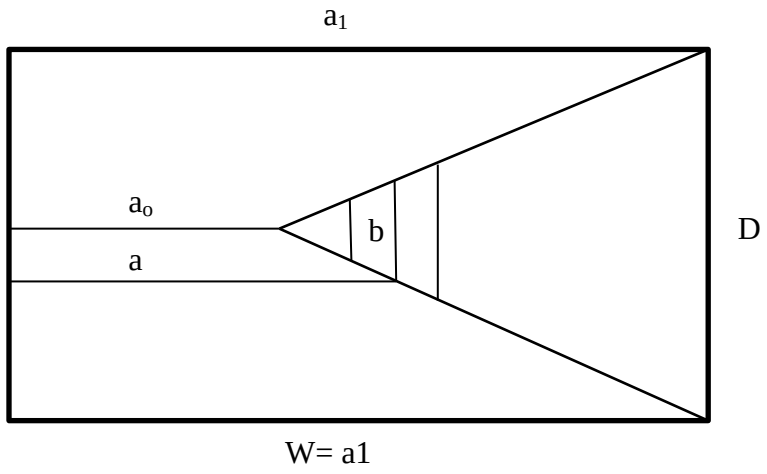

Figure 30: NTP specimen for FCP

As has been shown by Bubsey[55] and others[56-62], Y^* reaches a minimum value, which is dependent on specimen geometry only. During fracture toughness (K_{IC}) determination, the load

required to drive a crack reaches a maximum at the minimum value of Y^*. Since the stress intensity factor, K_I, is given by,

$$K_I = Y^* P/(D\sqrt{W})$$

Where

$$Y^* = \left(\frac{1}{2}\frac{dC}{d\alpha}\frac{\alpha_1 - \alpha_\circ}{\alpha_i - \alpha_\circ}\right)^{1/2}$$

K_I's magnitude, under constant load, will follow the same trend as Y*, i.e. it will first decrease to a minimum before starting to increase. This became obvious during the attempt to use the NTP specimen K_{IC} test for fatigue crack propagation (FCP) studies. Three Plexiglas specimens were tested and the results have been analyzed according to the guidelines of ASTM E647[49].

Specimen 1 and 2 had too few points to be "useful". Specimen 3 was adequate. The analysis of the results showed the expected behavior of Y* as a function of α, the normalized crack length (α=a/W). The behavior of Y* as a function of number of cycles, and therefore crack length, was paralleled by ΔK.

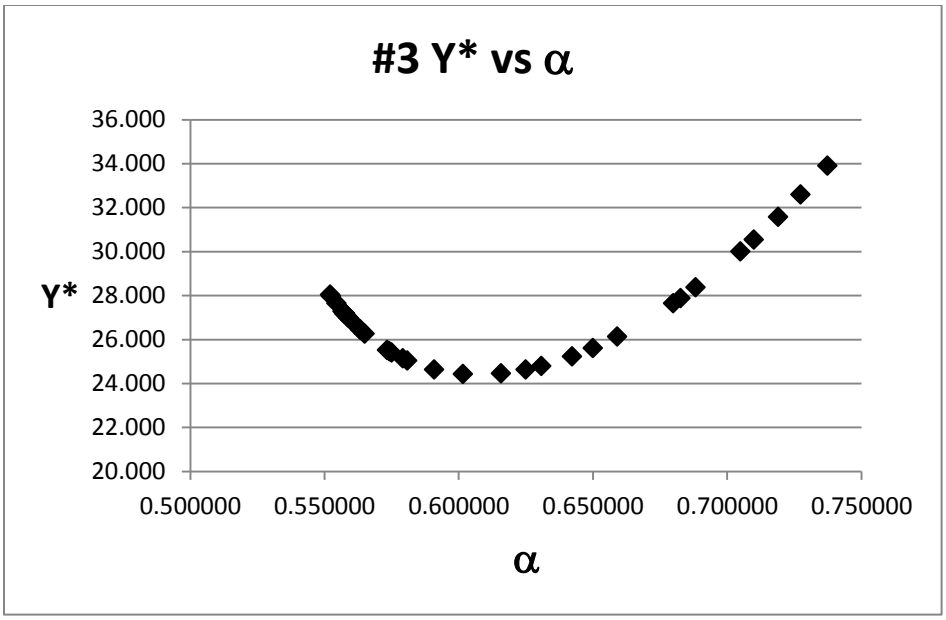

Figure 31: FCP Specimen #3 Y* vs a

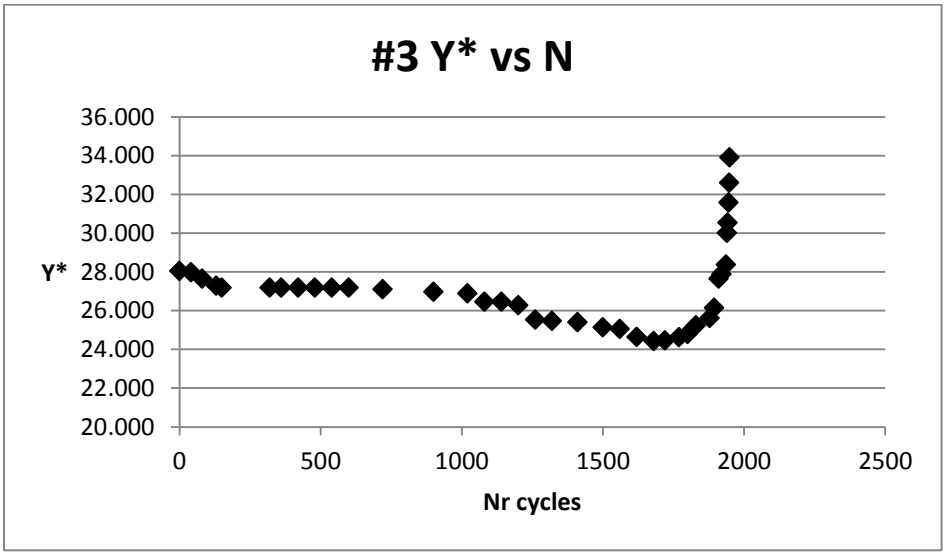

Figure 32: FCP Specimen #3 Y* vs N

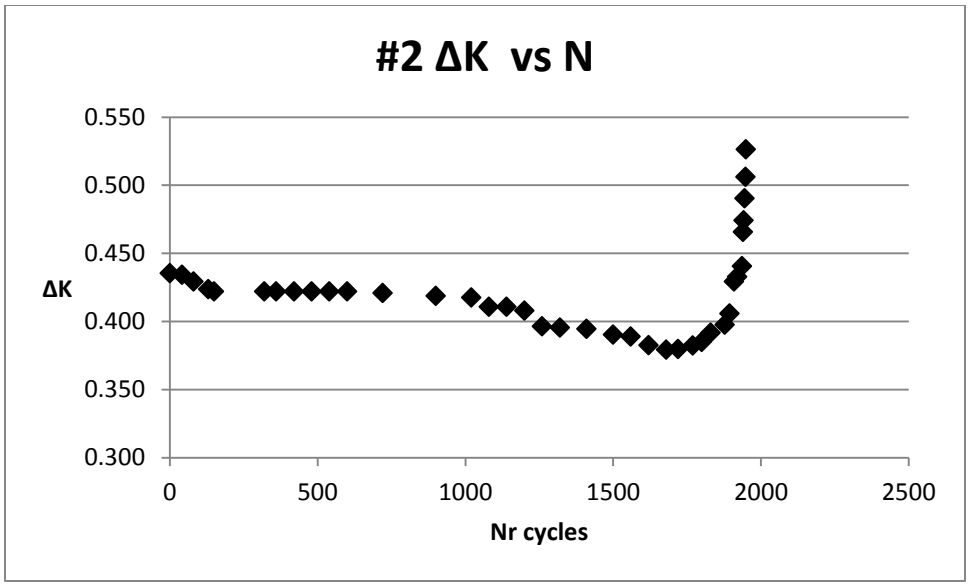

Figure 33: FCP Specimen #3 ΔK vs N

If only the data points that occurred after Y* (or ΔK) reached its minimum were considered, a characteristic FCP da/dN vs ΔK log/log curve could be obtained (see below). The slope of the curve, which is the exponent **m** in Paris' Law, is 13.5, a value which is close to values reported in the literature for poly(methyl methacrylate).[63]

At this stage, however, further research should be conducted to evaluate the feasibility of the NTP specimen K_{IC} test to be used for FCP studies.

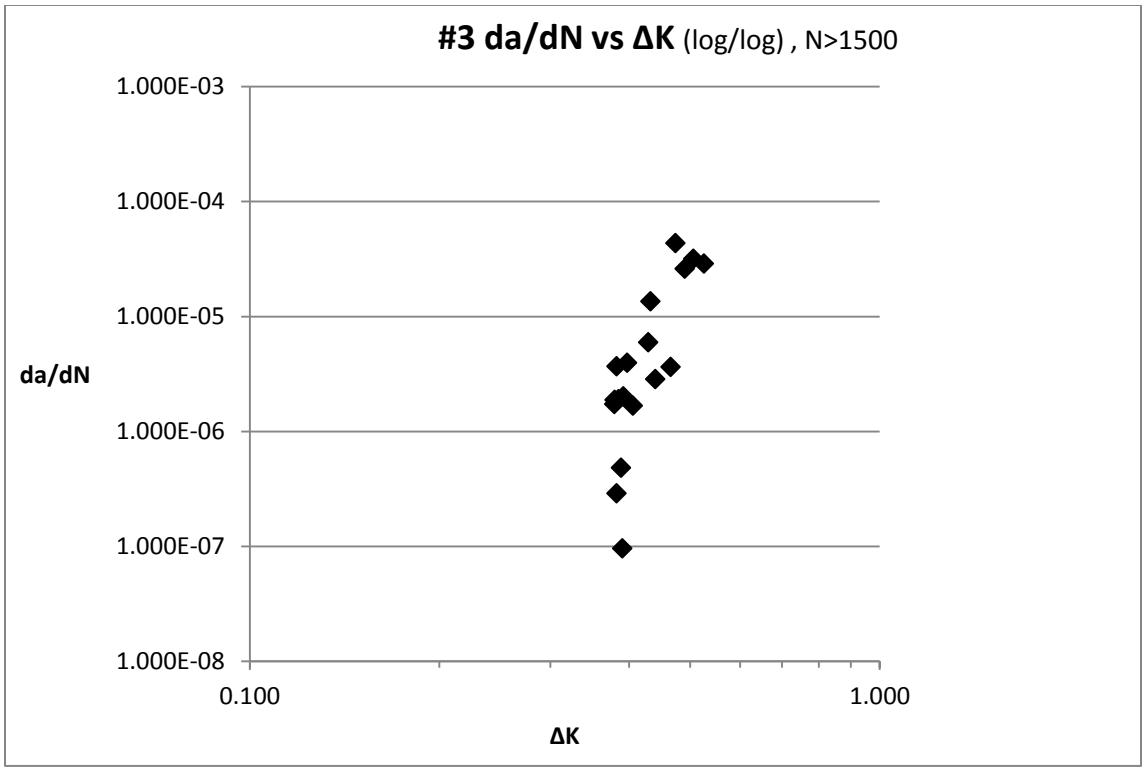

Figure 34: FCP Specimen #3 da/dN vs ΔK

Chapter 4: Conclusions

For fracture toughness, IPS e.max Press was found to be superior to IPS e.max CAD, therefore, the null hypothesis was rejected.

For the FCP test, experimental pilot specimens were tested to verify the methodology for testing FCP using the NTP specimen fracture toughness test. However, the results were inconclusive and further research is required to determine the feasibility of using a trapezoidal crack front such as the NTP specimen in fatigue crack propagation studies.

References

[1] Johnson WW. The history of prosthetic dentistry. J Prosthet Dent. 1959;9:841-6.

[2] Kelly J. Ceramics in restorative and prosthetic dentistry. Ann Rev Material Sci. 1997;27:443-68.

[3] Denry IL. Recent advances in ceramics for dentistry. Crit Rev Oral Biol Med. 1996;7:134-43.

[4] Conrad HJ, Seong WJ, Pesun IJ. Current ceramic materials and systems with clinical recommendations: a systematic review. J Prosthet Dent. 2007;98:389-404.

[5] Rekow ED. Dental CAD/CAM systems: a 20-year success story. J Am Dent Assoc. 2006;137 Suppl:5S-6S.

[6] Beuer F, Schweiger J, Edelhoff D. Digital dentistry: an overview of recent developments for CAD/CAM generated restorations. Br Dent J. 2008;204:505-11.

[7] Miyazaki T, Hotta Y. CAD/CAM systems available for the fabrication of crown and bridge restorations. Aust Dent J. 2011;56 Suppl 1:97-106.

[8] Miyazaki T, Hotta Y, Kunii J, Kuriyama S, Tamaki Y. A review of dental CAD/CAM: current status and future perspectives from 20 years of experience. Dent Mater J. 2009;28:44-56.

[9] Mormann WH. The evolution of the CEREC system. J Am Dent Assoc. 2006;137 Suppl:7S-13S.

[10] Andersson M, Razzoog ME, Oden A, Hegenbarth EA, Lang BR. Procera: a new way to achieve an all-ceramic crown. Quintessence Int. 1998;29:285-96.

[11] Bindl A, Mormann WH. Marginal and internal fit of all-ceramic CAD/CAM crown-copings on chamfer preparations. J Oral Rehabil. 2005;32:441-7.

[12] Smith WF. Principles of Materials Science and Engineering. 2 ed: McGraw-Hill Companies; 1990.

[13] Wray P. The American Ceramic Society. History of Ceramics (2009) Web 07-03-2014 <http://ceramicsorg/learn-about-ceramics/history-of-ceramics>.

[14] Kelly JR, Nishimura I, Campbell SD. Ceramics in dentistry: historical roots and current perspectives. J Prosthet Dent. 1996;75:18-32.

[15] McLean JW. The alumina reinforced porcelain jacket crown. J Am Dent Assoc. 1967;75:621-8.

[16] Kelly JR, Benetti P. Ceramic materials in dentistry: historical evolution and current practice. Aust Dent J. 2011;56 Suppl 1:84-96.

[17] Kelly JR. Dental ceramics: what is this stuff anyway? J Am Dent Assoc. 2008;139 Suppl:4S-7S.

[18] Barreiro M, Rlesgo O, Vicente E. Phase identification in dental porcelains for ceramo-metallic restorations. Dent Mater. 1989;5:51-7.

[19] Mackert Jr J, Butts M, Fairhurst C. The effect of the leucite transformation on dental porcelain expansion. Dent Mater. 1986;2:32-6.

[20] Isgrò G, Kleverlaan CJ, Wang H, Feilzer AJ. Thermal dimensional behavior of dental ceramics. Biomaterials. 2004;25:2447-53.

[21] McLaren EA, White SN. Glass-infiltrated zirconia/alumina-based ceramic for crowns and fixed partial dentures. Pract Periodontics Aesthet Dent. 1999;11:985-94.

[22] Kelly JR. Dental ceramics: current thinking and trends. Dent Clin North Am. 2004;48:513-30.

[23] Oilo M, Hardang AD, Ulsund AH, Gjerdet NR. Fractographic features of glass-ceramic and zirconia-based dental restorations fractured during clinical function. Eur J Oral Sci. 2014;122:238 - 44.

[24] Pieger S, Salman A, Bidra AS. Clinical outcomes of lithium disilicate single crowns and partial fixed dental prostheses: A systematic review. J Prosthet Dent. 2014;112:22-30.

[25] Ivoclar Vivadent | IPS e.max System. Web.19-6-2014. <http://www.ivoclarvivadent.us/emaxchangeseverything/system/>.

[26] VITA Innovation Professionals - Dentists. Web. 19-06-2014. <http://www.vita-vip.com/en/dentists/home>.

[27] Lava™ Frame Zirconia. Web. 19-06-2014. <http://solutions.3m.com/wps/portal/3M/en_US/3M-ESPE-NA/dental-professionals/products/category/digital-materials/lava-zirconia/>.

[28] Cercon® System. Web. 19-06-2014. <http://www.dentsply.ca/index.php?page=shop.product_details&flypage=flypage.tpl&product_id=34&category_id=64&option=com_virtuemart&Itemid=27>.

[29] Etman MK, Woolford M. Three-year clinical evaluation of two ceramic crown systems: a preliminary study. J Prosthet Dent. 2010;103:80-90.

[30] Kern M, Sasse M, Wolfart S. Ten-year outcome of three-unit fixed dental prostheses made from monolithic lithium disilicate ceramic. J Am Dent Assoc. 2012;143:234-40.

[31] Fasbinder DJ, Dennison JB, Heys D, Neiva G. A Clinical Evaluation of Chairside Lithium Disilicate CAD/CAM Crowns A Two-Year Report. J Am Dent Assoc. 2010;141:10S-4S.

[32] Anderson TL. Fracture mechanics: fundamentals and applications: CRC press; 2005.

[33] Dowling NE. Mechanical behavior of materials: engineering methods for deformation, fracture, and fatigue: Prentice Hall; 1993.

[34] Curtis RV, Watson TF. Dental biomaterials: imaging, testing and modelling: Elsevier; 2008.

[35] Ruse ND, Troczynski T, MacEntee MI, Feduik D. Novel fracture toughness test using a notchless triangular prism (NTP) specimen. J Biomed Mater Res. 1996;31:457-63.

[36] Barker L. A simplified method for measuring plane strain fracture toughness. Eng Fract Mech. 1977;9:361-9.

[37] Passos SP, Freitas AP, Jumaily S, Santos M, Rizkalla AS, Santos Jr GC. Comparison of mechanical properties of five commercial dental core build-up materials. Compend Contin Educ Dent. 2013;34:62-3, 5-8.

[38] Iwamoto N, Ruse ND. Fracture toughness of human dentin. J Biomed Mater Res A. 2003;66:507-12.

[39] Far C, Ruse ND. Effect of bleaching on fracture toughness of composite-dentin bonds. J Adhes Dent. 2003;5:175-82.

[40] Müller B, Pfrunder F, Chiocca L, Ruse ND, Beckmann F. Visualising complex morphology of fatigue cracks in voxel based 3D datasets. Mater Sci Technol. 2006;22:1038-44.

[41] Broek D. Elementary Engineering Fracture Mechanics Leyden, Netherlands: Noordhoff International; 1974.

[42] Gilbert C, Ritchie R, Johnson W. Fracture toughness and fatigue-crack propagation in a Zr–Ti–Ni–Cu–Be bulk metallic glass. Appl Phys Lett. 1997;71:476-8.

[43] Ritchie RO. Fatigue and fracture of pyrolytic carbon: a damage- tolerant approach to structural integrity and life prediction in "ceramic" heart valve prostheses. J Heart Valve Dis. 1996;5 Suppl 1:S9-31.

[44] Arola DD, Reprogel RK. Tubule orientation and the fatigue strength of human dentin. Biomaterials. 2006;27:2131-40.

[45] Arola DD, Rouland JA. The effects of tubule orientation on fatigue crack growth in dentin. J Biomed Mater Res A. 2003;67:78-86.

[46] Kruzic JJ, Nalla RK, Kinney JH, Ritchie RO. Mechanistic aspects of in vitro fatigue-crack growth in dentin. Biomaterials. 2005;26:1195-204.

[47] Scherrer SS, Cattani-Lorente M, Vittecoq E, de Mestral F, Griggs JA, Wiskott H. Fatigue behavior in water of Y-TZP zirconia ceramics after abrasion with 30μm silica-coated alumina particles. Dent Mater. 2011;27:e28-e42.

[48] Tsalouchou E, Cattell MJ, Knowles JC, Pittayachawan P, McDonald A. Fatigue and fracture properties of yttria partially stabilized zirconia crown systems. Dent Mater. 2008;24:308-18.

[49] ASTM. E647-05 Standard test method for measurement of fatigue crack growth rates. 2007.

[50] Carpinteri A, Paggi M. A unified interpretation of the power laws in fatigue and the analytical correlations between cyclic properties of engineering materials. International Journal of Fatigue. 2009;31:1524-31.

[51] Quinn JB, Quinn GD. A practical and systematic review of Weibull statistics for reporting strengths of dental materials. Dent Mater. 2010;26:135-47.

[52] Nohut S, Lu C. Fracture statistics of dental ceramics: Discrimination of strength distributions. Ceram Int. 2012;38:4979-90.

[53] Della Bona A, Mecholsky JJ, Jr., Anusavice KJ. Fracture behavior of lithia disilicate- and leucite-based ceramics. Dent Mater. 2004;20:956-62.

[54] Albakry M, Guazzato M, Swain MV. Fracture toughness and hardness evaluation of three pressable all-ceramic dental materials. J Dent. 2003;31:181-8.

[55] Bubsey R, Munz D, Pierce W, Shannon Jr J. Compliance calibration of the short rod chevron-notch specimen for fracture toughness testing of brittle materials. Int J Fract. 1982;18:125-33.

[56] Lai M, Lee K. KIC Determination using a chevron notched compact tension specimen. Eng Fract Mech. 1992;41:453-6.

[57] Sung J. On the plane strain and crack stability in chevron-notched specimen for kic and work-of-fracture determination. Eng Fract Mech. 1990;37:349-59.

[58] Boccaccini A, Rawlings R, Dlouhý I. Reliability of the chevron-notch technique for fracture toughness determination in glass. Mater Sci Engng A. 2003;347:102-8.

[59] Dlouhý I, Boccaccini A. Reliability of the chevron notch technique for fracture toughness determination in glass composites reinforced by continuous fibres. Scripta Mater. 2001;44:531-7.

[60] Barker L, Baratta F. Comparisons of fracture toughness measurements by the short rod and ASTM Standard Method of Test for Plane-Strain Fracture Toughness of Metallic Materials/E 399-78. J Test Eval. 1980;8:97-102.

[61] Barker L. Compliance calibration of a family of short rod and short bar fracture toughness specimens. Eng Fract Mech. 1983;17:289-312.

[62] Beech J, Ingraffea A. Three-dimensional finite element calibration of the short-rod specimen. Int J Fract. 1982;18:217-29.

[63] Molino L, Timmie Topoleski L. Effect of BaSO4 on the fatigue crack propagation rate of PMMA bone cement. J Biomed Mater Res. 1996;31:131-7.